Molecular Dynamics Simulation Study of Water in Amorphous Kapton

Grégory Marque,[†] Sylvie Neyertz,*[,†] Jacques Verdu,[‡] Valéry Prunier,[§] and David Brown[†]

LMOPS, UMR CNRS 5041, Université de Savoie, Bâtiment IUT, 73376 Le Bourget-du-Lac, France, LIM, UMR CNRS 8006, ENSAM, 151 Boulevard de l'Hôpital, 75013 Paris, France, and EDF R&D, Site des Renardières, 77818 Moret-sur-Loing, France

Received September 28, 2007; Revised Manuscript Received February 8, 2008

ABSTRACT: Molecular dynamics (MD) simulations of more than 40 model systems of dry and hydrated poly(pyromellitimide-1,4-diphenyl ether) (PMDA-ODA) polyimide, also known as Kapton, were undertaken in order to study the specific interactions between water and a glassy polymer matrix. Dry amorphous Kapton models were generated using a hybrid pivot Monte Carlo-MD single-chain sampling technique and were found to reproduce many features found experimentally. Water was subsequently introduced into the polyimide systems with weight percentages ranging from 1.4 to 10 wt % at 373 K. At the lower concentrations, water is found to occupy the pre-existing void space in the polymer matrix. On the other hand, there are significant changes in the volumetric, energetic, and conformational properties of the chains for water contents above ∼3%. The static and dynamic properties of the hydrogen bonds have been analyzed. In all cases under study, water is preferentially hydrogen-bonded to two sites, thus forming bridges. These water bridges, whose occurrence depends on the weight percentage of the penetrant, can link either two polymer sites, one polymer site and another water, or two other waters. Water clusters have been analyzed and found to be in agreement with findings from NMR, dielectric, and infrared attenuated total reflection (ATR) measurements. Their geometries are more chainlike and at high water contents approach a cocontinuous network. Such a characterization at the molecular level calls into question the commonly used interpretation of solubility curves based on the Zimm−Lundberg theory.

1. Introduction

Water absorption by polymers is largely studied because of the influence of water on the structural,[1,2] electrical,[3–5] and mechanical[6–9] properties of the polymers. Several theories have been proposed in the literature in order to characterize this phenomenon. For example, it has been suggested that absorption is mainly related to the void volume of the polymer.[10] On the other hand, water absorption has been directly correlated to the molecular formula of the polymer through a molar additive function of terms due to the constitutive groups of the monomer.[11] It is also possible to apply the classical thermodynamic approach of polymer–solvent miscibility.[11,12] Nevertheless, no real explanations of the underlying mechanisms have been provided by the aforementioned theories.[13] Another approach is to study sorption isotherms, that is, plots of water volume fraction as a function of water activity,[13–15] despite the fact that experimental characterizations do not always agree on the shape of the isotherms. This is the case, for example, for poly(pyromellitimide-1,4-diphenyl ether), also known as PMDA-ODA or Kapton (Figure 1).[16] At low activities, it is unclear whether there is a dual-mode sorption[17–21] or a quasi-linear moisture uptake versus relative humidity.[22–26] At high activities, some authors report a linear dependence[20,22–24,26] whereas others observe an upward curvature.[17–19,21,25] The latter has been interpreted by Yang and co-workers[17,18] in terms of water cluster formation by using equations derived from the Zimm−Lundberg theory.[27] However, dielectric measurements, NMR, and infrared attenuated total reflection (ATR) studies suggest the existence of water clusters at lower activities.[25,28–31] In addition, Yang et al. studied hygrothermally aged Kapton and found that it did not display the upwardly curving shape at high activities, which was interpreted by the authors as "the absence of clustering in the aged film" and was attributed to chemical modifications giving rise to more hydrophilic films.[18] This is difficult to understand as, at high activities, there is a lot of water to accommodate in the dense polyimide. In polyimides other than PMDA-ODA, water uptake is usually reported as being fairly close to a linear function of the relative humidity, but it is not always obvious either due to experimental uncertainities.[32]

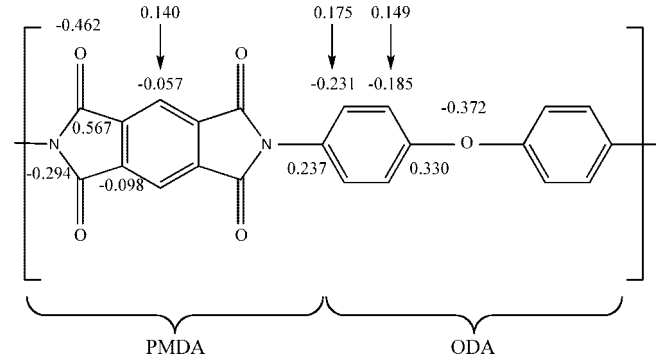

Figure 1. Kapton (PMDA-ODA) monomer with partial charges. Arrows point to charges carried by hydrogen atoms.

Within this context, it is interesting to attempt to complement experimental studies by using molecular dynamics (MD) simulations. Many MD studies of hydrated polar bulk polymers have now been reported in the literature. They include PA[33–35] or amide-based structures,[36–39] PMMA,[40] BPA-PC,[41] PVA,[41–49] and EVOH copolymers,[50] PEO[51–56] and PEO-based polymer electrolytes,[57,58] PBO,[59] perfluorinated ionomers,[60,61] poly(phenyl sulfones)[62] and sulfonated polyimides,[63] reverse micelles,[64–66] PE and PP,[67,68] epoxy resins,[69–71] novolac resins,[72] polyacrylates,[73] biodegradable polyesters,[74] or biopolymers.[75–77] They show that water interacts both with the polymer and with

* To whom correspondence should be addressed. E-mail: Neyertz@univ-savoie.fr.
[†] LMOPS, UMR CNRS 5041, Université de Savoie.
[‡] LIM, UMR CNRS 8006, ENSAM.
[§] EDF R&D.

10.1021/ma702173j CCC: $40.75
Published on Web 04/18/2008

other water molecules through hydrogen bonds and that it eventually moves within the matrix. However, the situation is often somewhat complicated. Goudeau et al.[34,35] propose that steric hindrance prevents water from accessing half of the hydrophilic amide groups in polyamide 6,6. In addition, they find water molecules bound to two hydrophilic sites as well as water clusters of a significant size (>10 molecules), even at low activities.[34,35] Some authors have also attempted to use molecular modeling techniques in order to study water solubility and, if possible, determine the water content at saturation in a polymer.[33,41,69,78–80] Their methods are based on a combination of the usual Widom test-particle insertion[81] with a thermodynamic integration,[33,41,78] a grid-search calculation,[69,82] or an excluded volume map sampling.[79,80]

Although a few MD simulations of short PMDA-ODA oligomers have been reported in the literature,[83–86] we are only aware of one study on long-chain amorphous Kapton.[87,88] However, the method used to create the chains is known to give a bias in the configurations due to the ever-increasing density that a growing chain end experiences.[89] Despite a complicated series of heating–cooling and compression–decompression cycles,[90] the density of this model attained only 95% of the experimental value.[88] This was attributed by the authors to errors in the parametrization,[88] but it may well be due in part to the poor choice of generation procedure.[91] We have previously studied the effect of 3.3 weight (wt) % water on short oligomers of PMDA-ODA and shown the coexistence of preferential sites for water on the chain backbones and water clusters.[85] These oligoimides were in the glassy state and were considered as a first approximation for their long-chain counterparts. However, the lack of experimental data on such short chains made it difficult to validate our models.

Here, we extend this study to the more realistic long-chain Kapton, both in the pure and in the hydrated states. The interaction potential is presented in Section 2. The pivot Monte Carlo-molecular dynamics (PMC-MD) technique[91–103] is validated for Kapton and used to generate realistic pure bulk models in Section 3. In Section 4, different weight percentages of water (from 1.4 to 10 wt %) are inserted into the polymer matrices. Changes in the volumetric and energetic properties, specific interactions between polymer and water, and the existence of water clusters are discussed as a function of the water content.

2. Interaction Potential

The force field for polyimides is basically the same as that described elsewhere[85,91,100,103] and will only be briefly outlined. The very high-frequency bond stretching modes are removed using rigid constraints,[104] which allows for the use of an integration time step of $\Delta t = 10^{-15}$ s and avoids problems with the equipartition of kinetic energy. The so-called "bonded" potentials include terms for restraining angle-bending and torsional rotations around the dihedral angles, as well as out-of-plane potentials to keep sp^2 structures planar. The "non-bonded" potentials are applied to all atom pairs belonging to different molecules and those on the same chain that are separated by more than two bonds. The van der Waals interactions between atoms of types i and j are of the Lennard−Jones (LJ) 12-6 form. The electrostatic potential is calculated using the Ewald summation method.[105,106] All polyimide−polyimide parameters were taken from the TRIPOS 5.2 force field,[107] while their partial charges (Figure 1) were obtained by performing *ab initio* calculations using the Gaussian computer program[108] at the B3LYP/6-31G** level.[100] Water potential parameters, including charges, were taken from the extended single point-charge model, SPC/E,[109] which is known to provide a good representation of bulk water.[110–112] In the same vein as most of the other simulations of hydrated polymers with the SPC/E model for water,[34–36,39,42,43,64,65,69,85] Lorentz–Berthelot combination rules[113] were used for van der Waals interactions. The MD simulations were performed using the gmq program[114] either in its scalar or in its parallel form on the Linux servers of the LMOPS and the University of Savoie as well as on the EDF "Rendvous" cluster in France.

3. Dry Kapton

3.1. Hybrid Pivot Monte Carlo-Molecular Dynamics (PMC-MD) Single-Chain Sampling. The hybrid PMC-MD method[91–103] was used to generate the starting configurations for PMDA-ODA, since it has already been validated for a variety of chains such as alkanes and PE,[92–94] PVC,[97] six different polyimides,[91,98,100,103] PEEK,[98] PBMA,[115] and cellulose.[116] In this approach, the configurational phase-space of the polymer is sampled using pivot Monte Carlo (PMC) moves[117,118] for rotatable torsions, while standard MD algorithms are used to explore the various oscillatory modes of the chains. The method is based on Flory's "local energy approximation";[119] that is, the hypothesis that polymer configurations in the pure melt are very similar to those obtained by sampling an isolated molecule, where only a certain number of specific near-neighbor intramolecular interactions are considered between atoms separated by no more than a fixed number of backbone bonds (n_{bonds}). Our experience using realistic potentials, and without any assumptions of ideality, is that this approach works very well for a large number of polymers,[91–103,115,116] among which are several polyimides with $n_{\text{bonds}} = 4$.[91,98,100,103] However, the value of n_{bonds} needs to be properly checked each time a new chemical structure is considered. The procedure to find and validate n_{bonds} is to compare the configurational and conformational properties of chains sampled by the PMC-MD method ("single-chain") with those of a fully interacting dense system of the same chains decorrelated by MD only ("bulk melt"). If the generation procedure is appropriate, the structural characteristics of both types of chains should be very similar. However, in order to decorrelate the bulk melt chains under a time scale accessible to MD simulations, this test generally needs to be carried out both at high temperature and on short oligomers. Since it has been shown that the test results are independent of chain size,[92–98,115,116] the assumption is that it should also be applicable to longer chains which cannot be relaxed with MD alone.

"Single-chain" PMDA-ODA test systems contained one 158-atom chain (4-mers) simulated for 20 000 ps at 1000 K, with the PMC-MD method and a preset value of n_{bonds}. The corresponding cubic "bulk melt" box contained 27 such oligomers run by MD for 15 000 ps under NpT conditions at 1000 K in which the isotropic pressure, p, is maintained at 1 bar by loose-coupling with a coupling constant of 5 ps,[120] and the temperature, T, is held constant by weak-coupling to a heat bath with a coupling constant of 0.1 ps.[121] Optimal convergence of the Ewald sum[122,123] was obtained using $\alpha = 0.3$ and $K_{\max} = 12$, while the real-space potential was truncated at $R_c = 8.5$ Å. The van der Waals potentials were also truncated at $R_{\text{vdW}} = 8.5$ Å, and long-range corrections to the energy and the pressure were applied.[113] In order to ensure that the chains were truly decorrelated from their initial configurations, the normalized autocorrelation functions for the end-to-end vector $\mathbf{R}_i$ of the individual chains as a function of time were calculated:

$$C_R(t) = \frac{\langle \mathbf{R}_i(0)\, \mathbf{R}_i(t)\rangle - \langle \mathbf{R}_i\rangle^2}{\langle \mathbf{R}_i^2\rangle - \langle \mathbf{R}_i\rangle^2} \tag{1}$$

The $C_R(t)$ for both single-chain and bulk melt chains are displayed in Figure 2. They show that decorrelation is indeed attained in both cases over the time scale considered despite

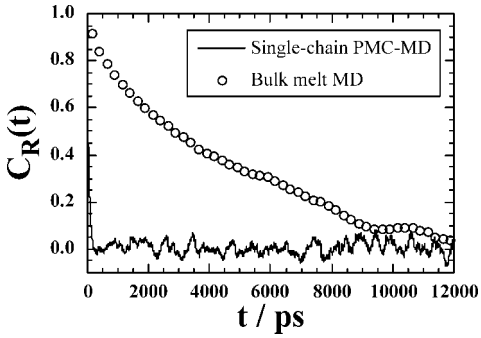

Figure 2. Normalized autocorrelation function for the end-to-end vectors, $C_R(t)$, of 158-atom PMDA-ODA chains, sampled both with single-chain PMC-MD (lines) and with full potential bulk melt MD (circles) at 1000 K.

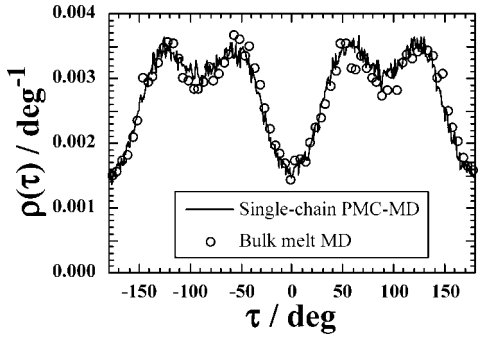

Figure 3. Single-chain-sampled (lines) versus bulk melt (circles) probability densities for the C−C−O−C τ pivot torsion angle in 158-atom PMDA-ODA chains using $n_{bonds} = 4$ at 1000 K.

the much longer decorrelation time in the MD simulation. The autocorrelation functions for significant dihedral angles and square end-to-end distances support this conclusion.

Figure 3 reports the distributions of the ODA C−C−O−C pivot torsion angle τ (see Figure 1) for both single-chain and bulk melt relaxed chains. They become superimposable for a value of $n_{bonds} = 4$. A similar level of agreement was found in the distributions of the mean-square end-to-end distances $\langle R^2 \rangle$, mean-square radii of gyration $\langle S^2 \rangle$, and the other pivot torsional angle, that is, the C−N−C−C link between the PMDA and ODA moieties (Figure 1). This clearly shows that the hybrid PMC-MD method with $n_{bonds} = 4$ is appropriate to generate starting Kapton configurations for the subsequent MD runs. PMC-MD calculations with different numbers of monomers ($n_{monomers}$) show that $\langle R^2 \rangle / n_{monomers}$ becomes number-independent from $n_{monomers} \sim 30$. A length of 50 PMDA-ODA monomers, amounting to 1952 atoms per chain, was thus chosen for the remaining studies.

3.2. Generation of Dense Kapton Models. Once generated by PMC-MD single-chain sampling in the melt (750 K), that is, above its glass transition temperature (~650–690 K),[20,26,124,125] uncorrelated PMDA-ODA chains are randomly reorientated and distributed in a periodic cubic MD box at an initial density close to the experimental value of ~1400 kg m^{-3}.[20,25,31,126–129] As described before,[91,98–100,103] a "phantom" atom is briefly placed at the center of mass of each 5-atom and 6-atom ring in order to avoid unphysical spearings and interlockings[130] during the introduction of excluded volume. The "bonded potentials" are then switched on. To remove the huge overlap energies of the initial structures, the excluded-volume potential is introduced very progressively during short MD simulations under constant-volume and temperature conditions (NVT). Phantom atoms are then removed, and electrostatic interactions are switched on. For long chain Kapton, the optimal

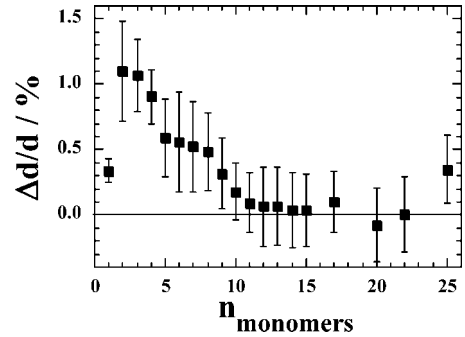

Figure 4. Average relative differences $\Delta d/d = (d_{PMC\text{-}MD} - d_{MD})/d_{PMC\text{-}MD}$ with their associated standard errors in the intramolecular distances between ODA ether oxygens separated by $n_{monomers}$: the chain configurations obtained at the end of the PMC-MD procedure are compared to the corresponding ones at the end of the full-potential equilibration for five 11712-atom polymer models at 750 K.

nonbonded parameters are $\alpha = 0.25$, $K_{max} = 11$, and $R_c = R_{vdW} = 9$ Å. Systems are then relaxed under NVT conditions at 750 K until thermal equilibrium is established; that is, the kinetic energy is equipartitioned between the different degrees of freedom. The bulk systems are then progressively cooled toward 300 K at a rate of -1 K ps^{-1}, relaxed for 100 ps at NVT, and then switched to constant-pressure (NPT) conditions, in which the on-diagonal and off-diagonal components of the pressure tensor, **P**, are maintained at ~1 and 0 bar, respectively, by a standard loose-coupling method where cell lengths and angles vary in time.[114] Systems were allowed to relax until the densities and energies stabilized. Production runs were then continued for, at least, another 600−1000 ps.

It has been shown in the past for *n*-alkane chains[92,94] and more recently for highly flexible bead-spring models[131] that the introduction of the full potential into an initially noninteracting ensemble of chains can lead to a change in the intrachain distances at intermediate length scales. In order to check whether our 50-mer PMDA-ODA chains are also affected, intermediate intramolecular distances between ODA oxygens were calculated both for the chain conformations obtained at the end of the PMC-MD sampling ($d_{PMC\text{-}MD}$) and following their equilibration in the 6-chain (11712-atom) bulks at 750 K (d_{MD}). Figure 4 reports the relative difference, $\Delta d/d = (d_{PMC\text{-}MD} - d_{MD})/d_{PMC\text{-}MD}$, averaged over five 11712-atom simulation boxes as a function of $n_{monomers}$. While there are slight deformations at intermediate distances, the average $\Delta d/d$ values are typically less than 1%, thus showing that, in the case of these relatively rigid PMDA-ODA chains, this effect remains very limited.

3.3. Validation of the Dry Kapton Model. The density of a simulated system is a fundamental property, since it results from the growth procedure, the accuracy of the force field, and the other parameters of the model. Moreover, most of the polymer properties, such as free volumes, are directly or indirectly linked to the density. The average densities at 300 K for nine 3904-atom and five 11712-atom dry polymer models are displayed in Table 1. They are within less than 1% of the experimental value, $\langle \rho^{300K}_{experiment} \rangle = 1399 \pm 4$ kg m^{-3}, obtained from the average of seven values found in the literature.[20,25,31,126–129] Using the coefficient of volumetric expansion for amorphous Kapton reported as being $\sim 1.92.10^{-4}$ K^{-1} between 300 and 373 K,[132] we can estimate $\langle \rho^{373K}_{experiment} \rangle$ as being equal to ~1380 kg m^{-3}. This differs by only 0.2% from $\langle \rho^{373K}_{model} \rangle = 1377 \pm 2$ kg m^{-3} (Table 1), which further validates our dry polymer models at 373 K.

The average total intermolecular potential energies $\langle U^{inter}_{pot} \rangle$ are also given in Table 1. In agreement with other long-chain polyimides,[99,100] the cohesive energies of the dry systems are mostly dominated (up to ~90%) by van der Waals interactions. $\langle U^{inter}_{pot} \rangle$

Table 1. Results of NPT Simulations Undertaken for Dry Kapton at 300 and 373 K and for Hydrated Kapton at 373 K[a]

systems	no. of atoms	$\langle\rho\rangle$	$\langle V\rangle$	$\langle U_{pot}^{inter}\rangle$	$\langle\delta\rangle$	$\langle$FFV$\rangle$	$\langle r_{0.5}\rangle$
dry 300 K (9 systems)	3904	1385 ± 7	45850 ± 230	-115.5 ± 0.9	20.5 ± 0.1	0.124 ± 0.005	3.10 ± 0.05
dry 300 K (5 systems)	11 712	1387 ± 2	137900 ± 200	-116.5 ± 0.4	20.56 ± 0.04	0.123 ± 0.001	3.10 ± 0.05
dry 373 K (5 systems)	11 712	1377 ± 2	138290 ± 150	-114.5 ± 0.5	20.31 ± 0.05	0.128 ± 0.001	3.10 ± 0.05
hydrated 373 K 1.4% wt H_2O (5 systems)	11 979	1397 ± 3	138310 ± 260	-129.0 ± 0.4			
hydrated 373 K 3.4% wt H_2O (5 systems)	12 360	1420 ± 2	138680 ± 150	-150.0 ± 0.3			
hydrated 373 K 5.4% wt H_2O (5 systems)	12 741	1438 ± 2	139660 ± 160	-171.5 ± 0.4			
hydrated 373 K 10% wt H_2O (5 systems)	13 617	1453 ± 4	144180 ± 360	-218.3 ± 0.6			

[a] All results have been averaged over the production runs and are presented with their standard errors. Average pressures in all systems were 1 ± 1 bar. The relaxed densities $\langle\rho\rangle$ are given in kg m^{-3}, and the volumes $\langle V\rangle$ of the MD cells are in $Å^3$. The potential intermolecular energies $\langle U_{pot}^{inter}\rangle$ are in kJ mol^{-1} (Kapton monomer)$^{-1}$, the Hildebrand solubility parameters $\langle\delta\rangle$ are in $(J\ cm^{-3})^{1/2}$, and the nearest-neighbor intermolecular distances $\langle r_{0.5}\rangle$ are in Å. $\langle$FFV$\rangle$ is the fractional free volume.

is directly linked to the average volume of the MD cell $\langle V\rangle$ and to the Hildebrand solubility parameter δ (Table 1) by:

$$\delta = \sqrt{\frac{\langle U_{pot}^{inter}\rangle}{\langle V\rangle}} \quad (2)$$

While there are several empirical techniques to evaluate Hildebrand solubility parameters,[11] these are rarely fully satisfactory. Indeed, the δ parameters for an ODPA-ODA homopolyimide were found to be 27.9 $(J\ cm^{-3})^{1/2}$ using the Hoy method,[133] 25.8 $(J\ cm^{-3})^{1/2}$ with the Fedors method,[134] and 21.4 $(J\ cm^{-3})^{1/2}$ with the Hoftyzer−van Krevelen method.[11,135] These shortcomings have been linked to the inability of the various group contribution approaches to take into account specific interactions. However, it is widely accepted that, as a requirement for a polymer to be soluble in a solvent, the absolute difference of their respective solubility parameters should be as small as possible.[11] As such, our model $\langle\delta\rangle = 20.5\ (J\ cm^{-3})^{1/2}$ at 300 K is in good agreement with the δ values of the solvents commonly used for PMDA-ODA. These solvents are typically H-bonding, and, as such, the hydrogen bonding contribution δ_h to the overall δ, $\delta^2 = (\delta_d^2 + \delta_p^2 + \delta_d^2)$, with δ_d and δ_p being the dispersive and polar contributions, respectively, is not negligible: $\delta = 22.7\ (J\ cm^{-3})^{1/2}$ and $\delta_h = 12.9\ (J\ cm^{-3})^{1/2}$ for m-cresol, $\delta = 22.9\ (J\ cm^{-3})^{1/2}$ and $\delta_h = 7.2\ (J\ cm^{-3})^{1/2}$ for *N*-methyl-2-pyrrolidone, $\delta = 22.8\ (J\ cm^{-3})^{1/2}$ and $\delta_h = 10.2\ (J\ cm^{-3})^{1/2}$ for dimethylacetamide, and $\delta = 24.9\ (J\ cm^{-3})^{1/2}$ and $\delta_h = 11.3\ (J\ cm^{-3})^{1/2}$ for dimethylformamide.[11]

Structures can be characterized in several ways. No sign of crystallinity was found in the indiscriminate intermolecular radial distribution functions for the chains $g_{inter}(r)$. They are in good agreement with the *d*-spacing parameters commonly reported for PMDA-ODA, that is, 4.45–4.6 Å.[126,136] The average nearest-neighbor intermolecular distances, $r_{0.5}$, arbitrarily defined as $g_{inter}(r_{0.5}) = 0.5$ show that the preparation procedure is fully repeatable. The distributions of pivot C−N−C−C angles show favored positions at −152°, −28°, 28°, and 152°, which agree with the Kapton ultraviolet spectrum.[137] The rotational barriers are much lower in the case of the more flexible C−O−C−C ether linkage, and the distributions are a lot smoother. As seen in the Kapton oligomers,[85] both dianhydride and diamine units can stack in a planar fashion, which leads to short-range order. The dianhydride−diamine interactions are especially relevant with respect to charge-transfer complexes (CTC),[125,138] which have been characterized in PMDA-ODA by UV/visible spectroscopy, fluorescence spectroscopy, and photoconductivity.[139] Although electrons cannot be formally transferred in classical MD simulations, CTC can only form if there is a sound structural basis for stacking. In addition, there are favored interactions between two dianhydride moieties, which are supposed to form low-energy configurations.[83,140]

The fractional free volume, FFV, available in the dry models can be empirically calculated using $FFV = (V - V_0)/V$, where V is the actual volume and V_0 is the zero point molar volume. The latter was taken as being 1.3 times the van der Waals volume V_w of the PMDA-ODA monomer calculated by a group contribution method.[11,141] From the simulated values at 300 K (Table 1), the $\langle$FFV$\rangle$ is 0.12, which compares favorably with the experimentally reported FFV of 0.11–0.12.[20,127,129] However, the way in which the void space is actually distributed remains experimentally unclear, as positron annihilation lifetime spectroscopy (PALS) is not able to provide such information. This has been attributed to the strong effective charges of the PMDA-ODA carbonyl oxygens and nitrogens (see partial charges in Figure 1), which are thought to trap positrons.[142] As such, we cannot use an approach whereby PALS spectra are directly compared to data obtained from atomistic simulations.[130,143,144] Instead, we use here a simpler geometric technique, referred to as the "phantom sphere approach" and widely encountered in atomistic simulations,[130,145–148] to characterize the void space. The probe accessible volume (PAV) is obtained by repeated trial insertions of virtual probes of preset radius into the dense polymer configurations without any preassumption on the actual form of the holes. Standard van der Waals radii are assumed for atoms in the polymer (C = 1.7 Å, O = 1.5 Å, N = 1.55 Å, and H = 1.2 Å), and the virtual probe insertions are "accepted" or "rejected" according to whether the probe overlaps with any of the atoms in the system. The accessible volume is then defined as the total volume of the system multiplied by the percentage of "accepted" insertions. It should be noted that the PAV is here that part of the volume that is accessible to the center of the probe. No attempt is made to obtain the actual volume the entire probe can access, as the holes can adopt complicated geometries and the probes can overlap in different ways. This fairly crude method is thus only intended as a way to compare different model systems under the same conditions.

In these calculations, the probe radius was set to 0.54 Å, so as to give a percentage of PAV equal to the FFV. As before,[149] the qualitative distribution of the PAV was obtained by analyzing the connectivity of the positions of accepted probe insertions. Effectively two accepted probes are considered to be linked, that is, in the same hole, if the distance between them is less than some arbitrary distance. Hole sizes are then obtained from a standard cluster analysis of the interconnected points. Here, the arbitrary distance linking the probe centers was also set to 0.54 Å. Results for the distribution of PAV (not displayed) show the monotonically decreasing form found for other glassy polymers.[144,148] Under those conditions, the small holes (i.e., PAV < 10 $Å^3$) are ∼30 times more numerous than the medium holes (10 $Å^3 \le$ PAV < 20 $Å^3$) and there are only few big holes (PAV ≥ 20 $Å^3$). No cavitation was observed. The distributions are also quite homogeneous between the different systems, which confirms the excellent reproducibility of the preparation procedure.

4. Hydrated Kapton

4.1. Water Insertion. While water molecules can be inserted randomly into the polymer,[34,35,37,38,40,41] this can lead to large

overlaps or even spearing in the case of cyclic molecules. Here, we use a more specific technique.[85] A sample of SPC/E water is equilibrated at a density of 958 kg m^{-3} at 373 K, that is, the experimental density of liquid water at the boiling point, in a simulation box of the same size as the preprepared dry polymer. After that, both simulation boxes are superimposed and the water molecules to insert are chosen among those that overlap least with the polymer atoms within a sphere of specified radius. The radius criteria and the initial water configurations can be changed in order to obtain different starting configurations for the water in the polymer matrix. However, providing that water mobility is sufficient, the results should not be dependent on the insertion technique. Following water insertion, a short step of minimization is needed to remove any slight overlaps. Systems are then ready to be simulated under NPT conditions.

Experimental measurements of the limiting weight percentage of water uptake by amorphous Kapton in contact with water vapor at its saturation pressure in the temperature range from 25 to 80 °C vary between ∼2% and ∼6%.[3,16,23–26,28–30,124,150–155] The scatter in experimental data is thought to be related to the film preparation history, the measurement technique, and in some cases the thickness of the films.[16,24,26,150] For example, Ree et al.[26] report a value of 3.4 wt % at 25 °C obtained by microbalance measurements. Given the experimental uncertainties, it was decided here to study a broader range of weight percentages: 0%, ∼1.4% (89 H_2O), ∼2.4% (152 H_2O), ∼3.4% (216 H_2O), ∼4.4% (279 H_2O), ∼5.4% (343 H_2O), ∼6.4% (406 H_2O), ∼8% (508 H_2O), and ∼10% (635 H_2O); figures in parentheses are the corresponding actual number of water molecules inserted into the dry polymer systems of 11 712 atoms.

It should be recalled here that, in a periodic model system, we are not limited to the amount of water that can be added to the polymer system, although phase separation is expected at very high water contents. On the other hand, in any real experiment, water in the polymer will be in equilibrium with some external water in a state with the same chemical potential. Although it may well be difficult, or even impossible, to obtain an external state of water with the same chemical potential at the highest concentrations examined here, there is, nevertheless, no fundamental reason to expect any discontinuities in the behavior with respect to water content because of this. The general trends are thus assessed here using a wider range of water contents than is experimentally accessible.

All five large 11 712-atom dry polymer models were used as starting points for the hydrated systems with 1.4%, 3.4%, 5.4%, and 10%. The 2.4%, 4.4%, 6.4%, and 8% simulations were carried out on one 11 712-atom system. Water mobility was characterized in a preliminary study. After 500 ps at 300 K, the water molecules were still not really decorrelated from their initial positions. On the other hand, heating the samples to 500 K led to a visible decorrelation of water from its initial distribution. Finally, a temperature of 373 K was chosen as a compromise in order to be both more experimentally realistic and still satisfactory in terms of water mobility. It has been shown experimentally that water concentration in Kapton is unchanged in the 30−85 °C temperature range and that it only depends on relative humidity.[23] Furthermore, with the heat of dissolution of water in Kapton being ∼−44 kJ mol^{-1},[23] the decrease of water solubility with temperature is almost entirely compensated by the increase of saturated vapor pressure, which indicates a low temperature effect on the water content at saturation.[156,157] All hydrated systems were simulated for 5000 ps, which was considered sufficient for the study of the structural properties of water in the polymer matrices. The Ewald parameters were $\alpha = 0.27$, $K_{max} = 13$, and $R_c = 9$ Å, and the total number of hydrated 11 712-atom model simulations

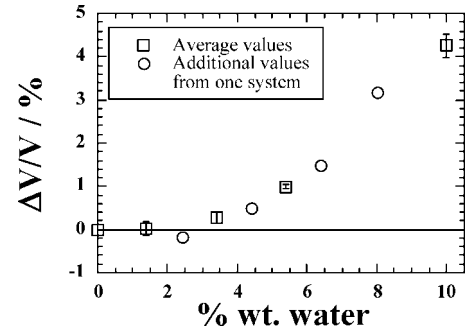

Figure 5. Average relative variations of the MD cell volumes $\Delta V/V = (V_{hydrated} - V_{dry})/V_{dry}$ as a function of the water content at 373 K. Those averaged over five hydrated systems are displayed with squares along with their standard errors. Circles give the additional average values obtained from a single system.

amounted to 24. Please note that all results presented for the water contents of 1.4%, 3.4%, 5.4%, and 10% are averaged over the five independent systems.

4.2. Volumetric and Energetic Properties. The average relative variations of the volumes $\Delta V/V = (V_{hydrated} - V_{dry})/V_{dry}$ at 373 K are reported in Figure 5 as a function of the water content.

Up to ∼3% wt water, the model volume remains basically equal to that of the dry sample, which suggests that water is likely to occupy pre-existing void spaces in the polymer. From ∼3% wt water onward, the hydrated volumes increase, but this cannot be explained by a direct correlation with the added volume of the water molecules. Indeed, the "volume occupied" by a single water molecule can be defined as the difference between the total probe accessible volume in a hydrated system using a probe of zero radius, with and without taking into account water, divided by the total number of water molecules. This analysis, at all wt % water, gives about 17 $Å^3$ per water molecule, that is, the same as that found using the same approach for a simulation box of pure liquid SPC/E water and as that used in other simulation studies.[34] It should be noted that this is significantly less than the ∼30 $Å^3$ obtained for the partial molecular volume of water from the density of liquid water.[110] This is not surprising, as our approach is based on a simple geometric notion of the volume "occupied" by a water molecule, whereas the partial molecular volume is the change in *total* volume of the system provoked by the addition of one more water molecule. For the hydrated polymer systems, the actual increases in total volume per water molecule are only equal to ∼4 $Å^3$ at 5.4% and ∼9 $Å^3$ at 10% wt water. This suggests that, even at the highest concentrations, there is still some way to go to reach the limiting value of ∼30 $Å^3$.

At the higher concentrations, the polymer matrix starts swelling, which is concomitant with changes in average model polymer–polymer distances and accessible void spaces. Figure 6 gives the average relative variations, $\Delta d'/d' = (d_{hydrated} - d_{dry})/d_{dry}$, of ODA oxygen intramolecular distances as a function of both $n_{monomers}$ and water content. There is a definite tendency toward an opening of the chains for the 5.4% and 10% systems for all analyzed intramolecular distances. Intermolecular distances tend to vary in the same direction.

Above ∼3% wt water, the PAV calculated without taking into account the penetrants also starts to increase, whatever the probe radius used in the insertion procedure. However, there are more small holes with respect to the dry samples. For example, in the 10% wt water systems, this amounts to a ∼35% increase in the amount of small holes when using the same probe radius and distance linking the probe centers of 0.54 Å as before. On the other hand, the larger holes tend to disappear for high

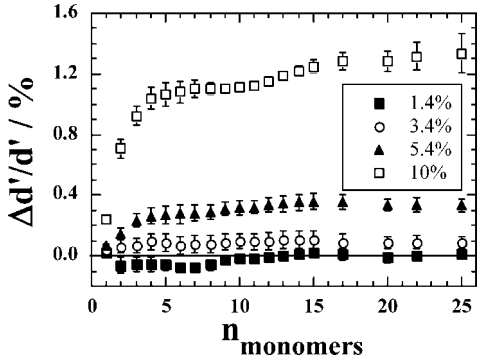

Figure 6. Average relative differences, $\Delta d'/d' = (d_{hydrated} - d_{dry})/d_{dry}$, with their standard errors in the intramolecular distances, d, between ODA ether oxygens separated by $n_{monomers}$: the hydrated ($d_{hydrated}$) systems are compared to the dry (d_{dry}) systems for various water contents at 373 K.

water contents. The fact that the extra volume is mainly created in the form of small holes suggests that the relaxation of the polymer induced by the presence of water is very local. This is also consistent with the geometries of the water clusters (see later).

The rather discontinuous behavior seen here of the volume first stagnating before beginning to swell over ~3% wt water (0.3% ± 0.1% change in volume at 3.4 wt %) warrants, perhaps, further comment. Previously, we have obtained 1.8% volume swelling of 4-mers of a very similar PMDA-ODA model at 300 K with 3.3% wt water.[85] This former result for short oligomers is more in agreement with the experimental results of Lim et al.,[25]who measured the density of just one type of Kapton at just one wt % (2.85%) at 23 °C and found a volume swelling of ~2.5%. However, several hygroscopic expansion coefficients for Kapton at room temperature[158,159] suggest that the volume expansion is actually at the most 0.6%–1% at high relative humidities (RH). This is corroborated by dilatometry measurements, which find a maximum of 0.7% volume swelling close to the saturation pressure at room temperature.[160] Furthermore, in the dielectric water sorption analysis of Giacomelli Penon et al.,[155] the change in sample thickness is deemed as being negligible in comparison with the increase in dielectric permittivity caused by the penetrating water. Most of the experimental data thus suggest that the swelling (up to saturation) remains very limited. It should also be noted that the time scale available to MD simulations is too short for the full range of natural glassy polymer relaxations to occur, and that it is not the first time a stagnation in the swelling behavior of glassy hydrated polymers has been seen; this is the case, for example, for PMMA, where swelling is thought to occur once free volume is saturated.[40] Within this context, our results on the volume changes in hydrated Kapton seem very reasonable.

As far as our model density is concerned, it increases as a function of water content (results not shown). Experimentally, density is often measured using density gradient columns, but, once again, there are no consistent trends in the literature for glassy polymers. Indeed, there are two limiting cases for these types of polymers: one assumes the sample volume does not change upon sorption of water, while the other assumes the mixture to obey volume additivity. In practice, the experimental data often lie between these limiting cases.[161] An increase in density has been reported for Kapton,[25] atactic PMMA,[162] PEEK,[163] the Matrimid polyimide,[161] bisphenol A-based polysulfone,[161] Nylon,[164] and aromatic polyamides.[165] In the case of starch[166] and isotactic PMMA,[162] an initial increase of density is seen at low RH, followed by a decrease at higher RH. Other experimental studies carried out on starch[167] and some sulfonated polyimides[168] report a decrease in density with water content. While different polymers may behave in different ways and the experimental conditions of the aforementioned references do vary, the most common case for glassy polymers and that reported for Kapton[25] does seem to be an increase in density with hydration, which is once again consistent with our model.

Polymer–polymer $\langle U^{inter}_{pol\text{-}pol}\rangle$, polymer–water $\langle U^{inter}_{pol\text{-}wat}\rangle$, and water–water $\langle U^{inter}_{wat\text{-}wat}\rangle$ intermolecular potential energies were extracted and are reported in Table 2. They were further resolved into their van der Waals ("LJ") and Coulombic ("Coul") contributions. As expected from the analyses shown previously, polymer–polymer interactions do not change much up to ~3% wt water. At larger water contents, the swelling leads to a limited increase in the $\langle U^{interLJ}_{pol\text{-}pol}\rangle$ and $\langle U^{interCoul}_{pol\text{-}pol}\rangle$ values, while there are no real variations in the overall intramolecular terms. In contrast, both the pol−wat and wat−wat interactions become more negative as an almost linear function of the water content. The pol−wat interactions are stabilized by both van der Waals and Coulombic terms, while the main contribution in the wat−wat energies is of electrostatic origin. With an entropy which is expected to increase with additional water, the results of Table 2 suggest that the uptake of water should be thermodynamically favorable at all the wt % values considered here. As noted before, this is hard to compare to experimental data because one would have to obtain an external state of water with the same chemical potential as the highest model concentrations.

4.3. Specific Interactions. Specific intermolecular radial distribution functions $g_{inter}(r)$ were calculated in order to characterize polymer−water and water−water interactions. As seen in other atomistic simulations,[34,35,37–39,42,44,45,47,50–53,55,59,60,62,64–66,70,71,73,85,169]the water hydrogens H_{wat} tend to form hydrogen bonds with the hydrophilic sites on the polymer, that is, for Kapton, the carbonyl oxygens O_{carb} and to a lesser extent the ether oxygens O_{eth} (Figure 7). This is consistent with the ^{13}C NMR study of Waters et al. where the carbonyl group was found to be the main interaction site for water on the polymer,[170] in contradiction to a much earlier work which had suggested the ether linkage.[23] In addition, there is a well-known correlation between water solubility and the concentration of polar groups in polyimides.[20] The other important hydrophilic sites are the oxygens from neighboring water molecules O_{wat}. Similar results are found if the $g_{inter}(r)$ functions are calculated with respect to O_{wat} instead of H_{wat}, albeit at distances larger by ~1 Å.

Hydrogen bonds can be defined using simple geometrical criteria.[34,36,42,44,47,53,59,70] This involves at least the distance between a H_{wat} and a hydrophilic site (A), but it can also use the value of the A···H_{wat}−O_{wat} angle. Our experience is that this last criterion is not really discriminating, and so we just use the experimentally quoted value of a hydrogen bond being defined each time a H_{wat} is less than 2.4 Å from a hydrophilic site ($d_{H\cdots O} \leq 2.4$ Å).[171] In addition, 2.4 Å corresponds to the distance of the first minimum in the $g_{inter}(r)$ for H_{wat}···O_{wat} and H_{wat}···O_{carb} (Figure 7). Our A···H_{wat}−O_{wat} angle distributions (not shown but accumulated in histograms of $\delta \cos\theta$ to avoid any bias) between hydrophilic sites and H_{wat}−O_{wat} identified as forming a hydrogen bond show a single Gaussian peak centered at 180°, and only 6% of A···H_{wat}−O_{wat} angles (those within the 125°–130° range) fall below the criterion of 130° used elsewhere.[34,45–47] The simple distance criterion described above is thus considered sufficient to detect hydrogen bonds, as was noted before for PEO.[53]

The H-bonding in the relaxed systems was analyzed with respect to each hydrogen atom in water and with respect to each water molecule using all three types of acceptors: O_{wat}, O_{carb}, and O_{eth}. This provided a large amount of information concerning the probabilities of occurrence of all the different possible combinations of H-bonds. To rationalize this information, we first present the data from the point of view of the water

Table 2. Average Polymer–Polymer (Pol−Pol), Polymer–Water (Pol−Wat), And Water–Water (Wat−Wat) Potential Energies for Dry and Hydrated Kapton at 373 K[a]

energies	dry (5 systems)	hydrated 1.4% wt H_2O (5 systems)	hydrated 3.4% wt H_2O (5 systems)	hydrated 5.4% wt H_2O (5 systems)	hydrated 10% wt H_2O (5 systems)
$\langle U^{inter}_{pol\text{-}pol}\rangle$	−114.5 (±0.5)	−114.4	−113.9	−113.2	−109.6
$\langle U^{interLJ}_{pol\text{-}pol}\rangle$	−104.2 (±0.4)	−104.4	−104.0	−103.4	−100.5
$\langle U^{interCoul}_{pol\text{-}pol}\rangle$	−10.2 (±0.3)	−10.0	−9.8	−9.8	−9.1
$\langle U^{inter}_{pol\text{-}wat}\rangle$		−10.3 (±0.6)	−22.7	−33.9	−56.1
$\langle U^{LJ}_{pol\text{-}wat}\rangle$		−1.7 (±0.5)	−4.3	−6.9	−12.6
$\langle U^{Coul}_{pol\text{-}wat}\rangle$		−8.6 (±0.4)	−18.3	−27.0	−43.4
$\langle U^{inter}_{wat\text{-}wat}\rangle$		−4.3 (±0.7)	−13.5	−24.5	−52.6
$\langle U^{LJ}_{wat\text{-}wat}\rangle$		1.1 (±0.1)	3.3	6.0	12.9
$\langle U^{Coul}_{wat\text{-}wat}\rangle$		−5.4 (±0.8)	−16.8	−30.5	−65.5

[a] Intermolecular $\langle U^{inter}\rangle$ energies are reported along with the specified van der Waals $\langle U^{LJ}\rangle$ and Coulombic $\langle U^{Coul}\rangle$ contributions in kJ mol^{-1} Kapton monomer^{-1}. The figures in parentheses give the maximum standard errors for each line.

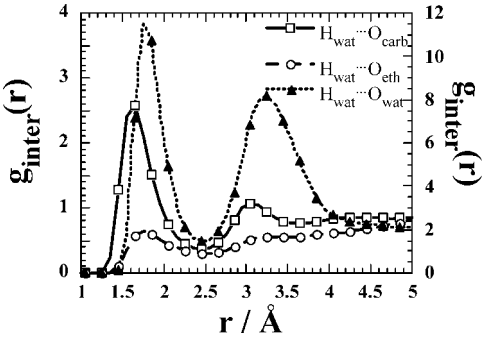

Figure 7. Intermolecular radial distribution functions $g_{inter}(r)$ between H_{wat} and different H-bond acceptor sites in a 3.4% system at 373 K. Note that the scale on the left axis is for the $H_{wat}\cdots O_{carb}$ and $H_{wat}\cdots O_{eth}$ rdfs and that on the right is for the $H_{wat}\cdots O_{wat}$ rdf.

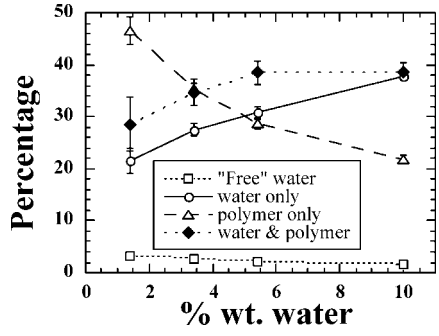

Figure 8. Percentages of the different types of water molecules plotted as a function of the water content (see text for details). The error bars are the standard errors from the five independent samples at each water content.

molecules by distinguishing four broad types of water: (1) "free" water, that is, water not H-bonded to any acceptor sites, (2) water only H-bonded to other water molecules, (3) water only H-bonded to acceptor sites on the polymer, and (4) water H-bonded both to other water molecules and to acceptor sites on the polymer. The change in the percentages of each type of water is presented as a function of the water content in Figure 8.

It is clear that the amount of free water is relatively low, even at 1.4% wt water, and that it decreases with water content. Most of the water molecules thus manage to form at least one H-bond with an acceptor site. At the lowest concentration studied, almost half of the water molecules are only H-bonded to O_{carb} or O_{eth} sites on the polymer chain. With increasing water content, the percentage of polymer-only H-bonded water molecules drops rapidly to ∼20% at the expense of their water-only and water and polymer counterparts. The steady increase in the amount of water-only H-bonded to other water molecules strongly suggests a trend toward water clustering, and this will be examined in more detail in a later section.

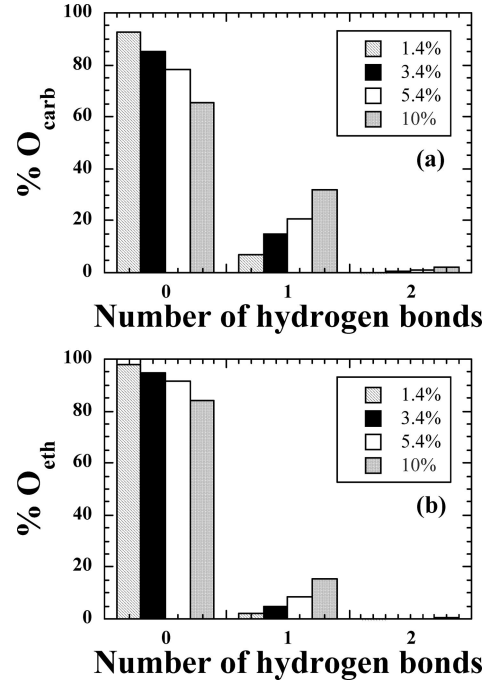

Figure 9. Distributions of the number of hydrogen bonds formed with water molecules at 373 K for the Kapton (a) carbonyl oxygens O_{carb} and (b) ether oxygens O_{eth}. Results are averaged over 5000 ps and five systems for each water content. The maximum standard error for a given water content is 0.6%.

We now consider the same data from the point of view of the O_{carb} and O_{eth} acceptor sites on the polymer. Although Figure 8 shows that the proportion of water H-bonded to the polymer gradually falls from ∼80% at 1.4% wt water to around 60% at 10% wt water, the actual number of polymer sites H-bonded to water gradually increases. Figure 9 shows the average percentages of polymer sites hydrogen-bonded with water as a function of the water content.

In the system with 89 water molecules (1.4% wt water), ∼88 carbonyl oxygens (∼7% of O_{carb}) and ∼6 ether oxygens (∼2% of O_{eth}) are hydrogen-bonded with a water molecule. As we have seen in Figure 8 though, only ∼75% of water molecules are H-bonded to the polymer chains at this water percentage. This suggests that a certain proportion of the water molecules are H-bonded to two sites, and this will also be examined in detail later. At 3.4% wt water, however, the 216 water molecules present are coordinated, at any one time, to ∼182 carbonyl oxygens (∼15% O_{carb}) and ∼15 ether oxygens (∼5% O_{eth}). So, despite the excess in the number of available coordination sites on the chain, some water molecules choose, as we will see in the next section, to coordinate preferentially to other water molecules. In this respect, Kapton behaves differently from the more hydrophilic polymers such as PVA and hydrogels where

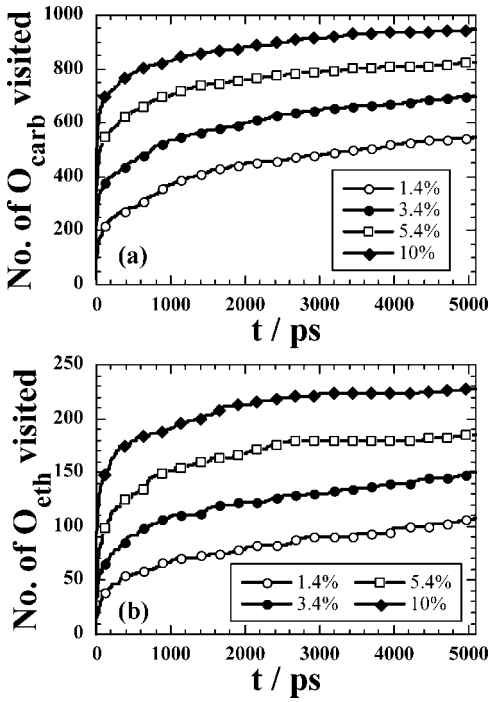

Figure 10. Average cumulative numbers of (a) O_{carb} and (b) O_{eth} which have formed at least one hydrogen bond with a water molecule plotted as a function of time for the different hydrated Kapton systems at 373 K. For reference, there are 1200 atoms of O_{carb} and 300 atoms of O_{eth} in each simulation box.

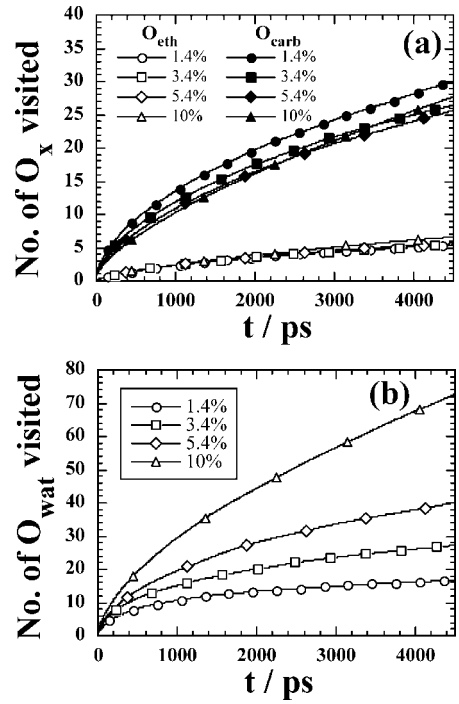

Figure 11. Average cumulative numbers of acceptor sites visited by a water molecule plotted as a function of time for the different hydrated Kapton systems at 373 K. The resolution is made into (a) O_{carb} (filled symbols) and O_{eth} (open symbols) sites on the polymer chain and (b) water oxygens. For reference, 1.4% = 89 H_2O, 3.4% = 216 H_2O, 5.4% = 343 H_2O, and 10% = 635 H_2O.

there is a higher average of water oxygens in the first solvation shell of a polymer oxygen.[42,45,47] This tail-off continues at higher water contents so that, at 10% wt with 635 water molecules, we find on average ~412 carbonyl oxygens and ~47 ether oxygens being hydrogen-bonded with a water molecule. This corresponds to only ~1/3 of the O_{carb} and ~1/6 of the O_{eth}. It has been suggested that this behavior could be simply due to the fact that some sites are inaccessible.[34] Yet, it is clear from Figure 10 that the cumulative numbers of hydrophilic sites that have formed, at least once, a hydrogen bond with a water molecule during the simulations increase steadily and are well above the instantaneous average values, which can be inferred from Figure 9. This weakens the hypothesis of inaccessible sites, although the duration of these simulations is too short to assess whether all sites can actually be visited.

The analyses shown in Figure 10 have also been made from the standpoint of the water molecules. In Figure 11, we plot the average cumulative number of different acceptor sites visited by a water molecule during the course of the simulation. These functions gradually increase with time, which demonstrates clearly that the water molecules do visit a number of different sites within the time span of the simulation. For the acceptor sites on the polymer (Figure 11a), there is, within the error bars (not shown for the purpose of clarity), little variation with the water content. The actual underlying distributions (not shown) are quite broad, symmetric, and roughly Gaussian. For example, at 10% wt water, some molecules manage to visit more than 60 O_{carb} during the simulation whereas others visit very few. It is also noticeable that the water molecules visit about 5 to 6 times as many carbonyl oxygens than ether oxygens in the same amount of time. This ratio is quite different from the static probabilities, which, as discussed above, are typically in excess of 10:1 in favor of carbonyl oxygens but are closer to the limiting value of 4:1, that is, the ratio of the number of carbonyl to ether oxygens in the systems. This suggests that visits to O_{eth} are shorter than those to O_{carb} (see H-bond lifetime analyses).

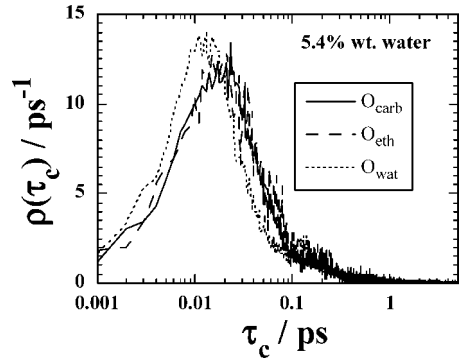

Figure 12. Probability densities of continuous H-bond lifetimes in a hydrated Kapton system with 5.4% wt water. H-bonds between water hydrogens and different types of acceptors have been considered. Note that the *x*-axis is on a logarithmic scale so as to better visualize the maximum at short times.

Figure 11b gives the average cumulative number of water oxygens that have formed an H-bond with a water molecule. The influence of the total water content of the samples is clearly quite different. In this case, increasing amounts of water lead to, in absolute terms, an increased number of water–water encounters. The reconciliation of this behavior with the absence of a water content effect for the number of polymer acceptor sites visited is that the increase in the number of water–water encounters occurs within water clusters, that is, within the increasing proportion of water which is only H-bonded to other water molecules (Figure 8). To put things in proportion, carrying out the same analysis for a simulation of pure SPC/E liquid water at 373 K gives a water–water encounter rate of ~170 molecules per 1000 ps.

The dynamics of the H-bonds were also analyzed in two other standard ways. First, continuous lifetimes τ_c of individual H-bonds were measured[36,43,45,47,56,70] and used to calculate both

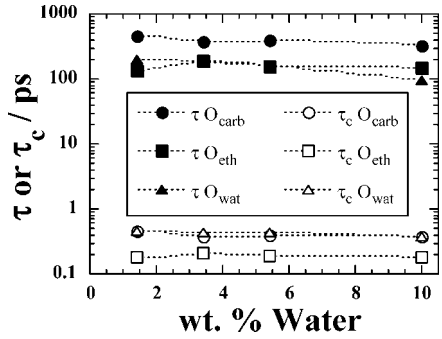

Figure 13. Mean values of the continuous H-bond lifetimes, τ_c, and H-bond correlation times, τ, as evaluated from eq 6, plotted as a function of the water content. Note the logarithmic scale on the *y*-axis. The maximum standard errors are 0.013 ps for τ_c and 50 ps for τ.

an average lifetime and a distribution of lifetimes, $\rho(\tau_c)$, for each specific type of H-bond. As pointed out previously,[47] this analysis is not without its drawbacks if it is made using stored configurations. Infrequent storage limits the resolution at low lifetime values, whereas a higher frequency will often cause practical problems with respect to file space. Results can be very sensitive to the actual definition of an H-bond,[172] and long-lived H-bonds may be either missed or, at best, truncated if the duration of the simulation is too limited. Nevertheless, it has been shown by Tamai et al.[43] using a resolution of 0.01 ps that a significant proportion of continuous lifetimes in a series of hydrogels are quite short. In order to resolve this short time behavior in our hydrated Kapton models, we have carried out extra simulations of 50 ps with the configurations being stored at every 1 fs time step. Averages were obtained at four different concentrations of water: 1.4, 3.4, 5.4, and 10% wt water. Typical results for the corresponding $\rho(\tau_c)$ obtained in a 5.4% system are plotted in Figure 12.

The high resolution used here for $\rho(\tau_c)$ shows that there is a maximum probability for the lifetimes in the region of 0.01−0.03 ps. The distributions for H-bonds with O_{wat} are slightly offset toward lower lifetimes compared to those for acceptors on the polymer chain, but 1 ps seems to be a long continuous lifetime whatever the type of H-bond.

As noted before, one should remain cautious, as the results are indeed found to be sensitive to the definition of an H-bond. Increasing the cutoff for the H···A distance to, for example, 2.6 Å significantly reduces the mean lifetimes, as there are a larger number of short lifetimes. In fact, it is found here that the value of $d_{H\cdots O} = 2.4$ Å maximizes the continuous lifetimes for all types of H-bonds. On the other hand, Figure 13 shows that the average τ_c lifetimes (using the H-bond defining distance of $d_{H\cdots O} \leq 2.4$ Å) are clearly relatively insensitive to the amount of water present. The fact that the H-bond τ_c values involving O_{eth} are approximately half of those with O_{carb} or O_{wat} is presumably due to the less negative charge of the ether site (see Figure 1).

Another well-known problem with the continuous lifetime analysis is that it does not give any information about the reforming of the same H-bond. The standard approach[59] to characterizing such an eventuality is a correlation function analysis.[172,173] A function is defined for each pair *ij* of possible H-bond donors and acceptors, which just takes the values 1 and 0 according to whether an H-bond is present between them. In our case, this is simply based on their distance apart at time *t*, $r_{ij}(t)$, in the following way:

$$H\{r_{ij}(t)\} = 1 \quad \text{if} \quad r_{ij}(t) \leq d_{H\cdots O} \tag{3a}$$

$$H\{r_{ij}(t)\} = 0 \quad \text{if} \quad r_{ij}(t) > d_{H\cdots O} \tag{3b}$$

The autocorrelation function $R(t) = \langle H\{r_{ij}(0)\}\ H\{r_{ij}(t)\}\rangle$ then gives a different measure of the time required for an H-bond to decay. In practice, we obtain this characteristic time for each type of H-bond from the normalized form of $R(t)$, which we refer to as $C(t)$.[47] The normalization is straightforward for these types of functions that only take values of 1 and 0 as $R(0) = \langle H\{r_{ij}(0)\}\ H\{r_{ij}(0)\}\rangle = \langle H\{r_{ij}(0)\}\rangle$:

$$\begin{aligned} C(t) &= \frac{R(t) - \langle H\{r_{ij}(0)\}\rangle^2}{\langle H^2\{r_{ij}(0)\}\rangle - \langle H\{r_{ij}(0)\}\rangle^2} \\ &= \frac{R(t) - \langle H\{r_{ij}(0)\}\rangle^2}{\langle H\{r_{ij}(0)\}\rangle - \langle H\{r_{ij}(0)\}\rangle^2} \\ &= \frac{R(t) - R^2(0)}{R(0) - R^2(0)} \end{aligned} \tag{4}$$

The normalized $C(t)$ function thus gives the probability of an H-bond still existing between two atoms at some later time, given that it did exist at the time origin. As it could have been broken and reformed several times in the intervening time, it does not give the same information as the continuous lifetime analysis. We note in passing that the normalized form that has been given in the past, $C(t) = R(t)/R(0)$,[36,43,45,47,56,70,172] is not strictly correct, since the long time limit is $R(0)$ rather than 0. However, as $R(0)$ is generally small compared to 1, this is not usually a problem.

The resulting $C(t)$ values all showed a similar behavior with an initial fast, highly nonexponential relaxation giving way at long times to a slow exponential decay. This is qualitatively very similar to that found for water in PVA[47] and water in epoxy−amine networks.[70] The combination of both of these quite different behaviors has posed problems in the past to obtain correlation times. Some authors have fitted the short time relaxation to a single exponential,[36,43] despite its clear nonexponential form, or simply defined the correlation time as $C(\tau) = 1/e$.[70] We have not found these approaches satisfactory, nor the alternative of fitting a stretched exponential, also known as KWW (Kohlrausch–Williams–Watts), form.[47] On the other hand, satisfactory fits to the data out to at least 3 ns were obtained using a weighted sum of a single exponential and a stretched exponential:

$$C(t) = \lambda \exp\left(-\frac{t}{\gamma}\right) + (1-\lambda)\exp\left(-\left(\frac{t}{\alpha}\right)^{\beta}\right) \tag{5}$$

The corresponding relaxation times, τ, could then be obtained from the best-fit values of the λ, γ, α, and β parameters and the analytical integration of eq 5:

$$\begin{aligned} \tau &= \int_0^\infty C(t)\,dt \\ &= \int_0^\infty \lambda \exp\left(-\frac{t}{\gamma}\right) + (1-\lambda)\exp\left(-\left(\frac{t}{\alpha}\right)^{\beta}\right) dt \\ &= \lambda\gamma + (1-\lambda)\frac{\alpha}{\beta}\Gamma\left(\frac{1}{\beta}\right) \end{aligned} \tag{6}$$

where the gamma function, $\Gamma(x)$, was estimated to high precision using a standard numerical technique.[174]

The values of τ obtained for H-bonds with the three types of acceptor sites are displayed as a function of water content in Figure 13. They fall in the same range, 10^2-10^3 ps, as that found for water in PVA at 375 K and at similar weight fractions.[47] They are considerably longer than the ∼6 ps correlation times obtained for pure SPC/E water at 373 K. In this study, the τ correlation times for O−H···O_{wat} and O−H···O_{eth} are roughly similar, whereas those for the O−H···O_{carb} H-bonds are about twice as long. The difference between O_{carb} and O_{eth} can once again be linked to the lower partial charges of O_{eth} with respect to O_{carb}. In the case of the O−H···O_{wat} H-bond, it is likely that the higher mobility of water counteracts its inherent strength and, on average, correlation times are less long than

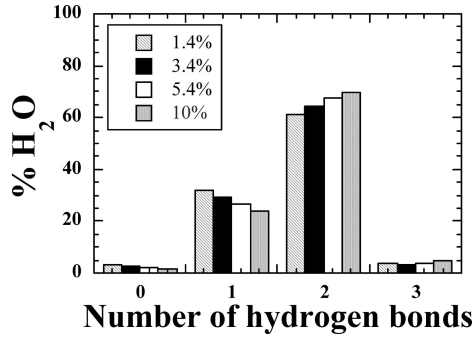

Figure 14. Distributions of the number of hydrogen bonds formed by one water molecule at 373 K. Results are averaged over 5000 ps and five systems for each water content. The maximum standard error for a given water content is 0.7%.

those for polymer–water interactions. Interestingly, we do not find the same phenomenon when looking at the short-time τ_c, as the strong O−H···O_{wat} H-bond augments its continuous lifetime with respect to that for the weaker O−H···O_{eth} H-bond. The fact that τ and τ_c might at least partially depend on different factors is not unexpected, as there are about 3 orders of magnitude of difference between both characteristic times for the same H-bond type (Figure 13). For both τ and τ_c, though, a definite trend with increasing water content is not obvious over the relatively narrow range of hydrations used here. Nevertheless, the results are not inconsistent with findings from MD simulations over much wider ranges of water content for more hydrophilic PVA hydrogels[47] or PEO solutions,[56] where increasing water content leads to clear decreases in H-bond correlation times.

4.4. Water Bridging. The average number of A···H−O hydrogen bonds per water molecule is displayed for several water contents in Figure 14.

Very few waters are either not bound to any or bound to three hydrophilic sites at the same time, suggesting that these are unfavorable states. On the other hand, a large majority of water molecules (from 60% to 70%) are hydrogen-bonded to two hydrophilic sites, in agreement with what has been proposed by experimentalists[13,14] and seen in other simulations of hydrated polymers.[34,51,53] As shown in Table 3, these so-called "water bridges" can link either two polymer sites ("P−W−P bridges"), two other water molecules ("W−W−W bridges"), or one polymer site and another water molecule ("P−W−W bridges"). The preferential polymer sites are the protruding O_{carb}, which can either form P−W−P O_{carb}−water−O_{carb} and P−W−W O_{carb}−water−O_{wat} bridges or combine to a lesser extent with O_{eth} to form P−W−P O_{carb}−water−O_{eth} bridges. In general, the O_{eth} show the same trend as the O_{carb} but are attenuated by their much lower accessibility with almost no P−W−P O_{eth}−water−O_{eth} and a few P−W−W O_{eth}−water−O_{wat} bridges. Unlike what has been found for flexible polymers such as PEO- or PEG-based surfactants,[52,53,64,65] there are actually very few intramolecular P−W−P bridges: less than 0.5% of the O_{carb}−water−O_{carb}, less than 0.02% of the O_{carb}−water−O_{eth}, and 0% O_{eth}−water−O_{eth} imply two sites on the same PMDA-ODA chain, irrespective of the water content. This is clearly related to the fact that the O_{carb} on the same PMDA moiety are over 5.5 Å apart and about as far from the closest O_{eth}. The rigid nature of the polyimide monomers makes it virtually impossible for these atoms to be bridged by a water molecule, and thus, over 99.5% of the P−W−P bridges are actually intermolecular. We do find some "cyclic bridges" where both hydrogens from the same water molecule form a loop with only one acceptor, but this involves at the most in all the simulations under study 0.6% of the O_{carb} and less than 0.05% of the O_{eth} and O_{wat} sites. Interestingly, the P−W−W bridges are by far the most common occurrence over 3.4% (and as many as the P−W−P bridges in the 1.4% systems), which suggests that it is easier for a water molecule coordinated to a polymer site to bridge with another water. Their number increases linearly with water content, which is consistent with the increase in the number of carbonyl oxygens and ether oxygens H-bonded to water (see Figure 9) and the linear decrease of the polymer–water interaction energy. The P−W−P and W−W−W bridges also display a quasi-linear increase of their average number with water content, but the evolution of their percentages show that the latter progressively replace the former at the higher concentrations. This is consistent with the swelling behavior seen in Figures 5 and 6. Proportionally, water tends to coordinate more and more to itself, thus eventually forming larger W−W−W networks at 10%.

4.5. Water Clusters. In the literature, several experimentalists[13,17,18,25] use the Starkweather interpretation[15] of the Zimm−Lundberg theory[27] in order to exploit solubility curves. In this approach, the linear part of the water volume fraction versus water activity curve is interpreted as the homogeneous dissolution of the water molecules in the polymer without formation of clusters, whereas the deviation of the curve at high activities is thought to be related to the clustering of water molecules.[13,15] According to this interpretation, clusters should thus not be present in Kapton, except at very high activities (see Introduction).[17] However, this contradicts NMR, dielectric, and infrared ATR studies.[25,28–31]

We have analyzed the clusters in our hydrated Kapton models by using the aforementioned hydrogen bond criterion ($d_{H\cdots O} \leq$ 2.4 Å) for defining water clusters, that is, water molecules which are hydrogen-bonded together. Average results obtained from the MD simulations for the 1.4% system are displayed in Figure 15a in the form of a histogram of the total amount of water contained in clusters of a given size. For comparison, we have also calculated the distributions of clusters in subsets of 89 water molecules (i.e., as many as in the 1.4% wt samples), selected in two other ways from samples of pure bulk water of the same size as the polymer samples. The first method was to just choose purely at random 89 water molecules and then perform the cluster analysis. Repeating this procedure many times gave an average distribution (not shown) containing mostly (∼93%) individual molecules with relatively small amounts of water in clusters. A second distribution, plotted in Figure 15a, was obtained for the as-inserted water. These latter results were generated from the initial configurations of hydrated polymer obtained using the method described in section 4.1. All five polymer samples were used, and the results were averaged over 10 superimpositions of independent water configurations in each case.

The MD relaxed and as-inserted distributions at 1.4% wt water, shown in Figure 15a, are quite similar. This seems to confirm the general impression that the water initially occupies the existing voids without disrupting the polymer, and suggest that more than ∼70% of the water molecules present are involved in clusters of one sort or another even at the lowest concentration studied. The same comparisons have also been carried out at higher concentrations. Results for 3.4% wt water are displayed in Figure 15b as it illustrates a trend seen for all the concentrations >1.4% wt water. At these higher concentrations, the percentage of isolated water molecules in the relaxed MD samples is systematically less than that found in the as-inserted ones. This suggests that the water does have an inherent tendency to alter the initial cluster distribution once allowed to relax. It will be shown later that this is not the only difference.

The fact that water clusters are present at low water contents apparently disagrees with the interpretation of the solubility

Table 3. Water Bridges between Two Hydrophilic Sites[a]

bridge type	% water	⟨no. of bridges⟩	percentage for a specific % water	bridge type	% water	⟨no. of bridges⟩	percentage for a specific % water
P−W−P O_{carb}−water−O_{carb} (±3, ±2)	1.4	24	40	P−W−W O_{carb}−water−O_{wat} (±4, ±1)	1.4	24	40
	3.4	42	27		3.4	70	46
	5.4	55	21		5.4	122	48
	10	78	16		10	226	45
P−W−P O_{carb}−water−O_{eth} (±0.9, ±0.5)	1.4	2.8	4.6	P−W−W O_{eth}−water−O_{wat} (±0.7, ±0.5)	1.4	2.2	3.6
	3.4	6.3	4.1		3.4	6.7	4.4
	5.4	9.1	3.6		5.4	13.3	5.2
	10	15.9	3.2		10	26.8	5.4
P−W−P O_{eth}−water−O_{eth} (±0.2, ±0.1)	1.4	0.1	0.2	W−W−W O_{wat}−water−O_{wat} (±4, ±2)	1.4	7	12
	3.4	0.3	0.2		3.4	28	18
	5.4	0.4	0.2		5.4	57	22
	10	1.0	0.2		10	152	30

[a] P refers to a polymer site, and W refers to a water site. The bridges have been analyzed over 5000 ps at 373 K both as a function of water content and as a function of the hydrophilic sites being either O_{carb}, O_{eth}, or O_{wat}. Results for each specific bridge type and each water content include the average number of bridges in the simulation cells and its total percentage with respect to the other bridge types. Their respective maximum standard errors are displayed in parentheses next to the name of the bridge. The number of intramolecular P−W−P bridges found is very small and never more than 0.5% of the total.

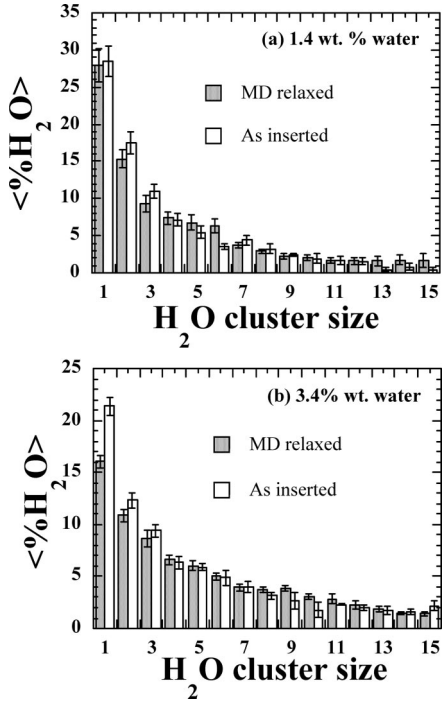

Figure 15. Average percentage of water molecules in clusters of a given size in the (a) 1.4% wt water and (b) 3.4% wt water systems at 373 K, along with the associated standard errors. The MD relaxed results are compared to those for the as-inserted water molecules (see text for details).

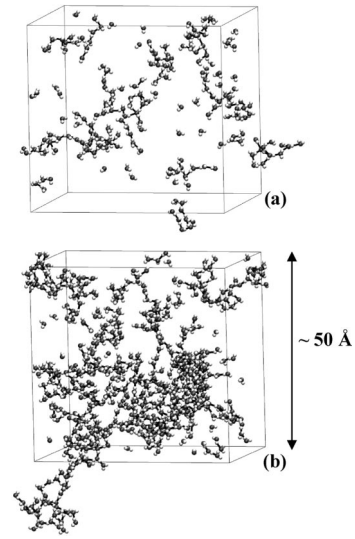

Figure 16. Schematic representations of the water clusters and their hydrogen bonds in (a) a 3.4% system and (b) a 10% system. The polymer is not shown, and the atoms are not folded back into the periodic box in order to better visualize the extent of the clusters. The images were generated using VMD 1.8.2.[176]

curves presented above. Furthermore, clusters can be much larger than two or three water molecules, that is, in agreement with what has been found in MD simulations of other polymer matrices.[34,36,42,47,50,60,61,67,68,72] The origin of the discrepancy between the aforementioned experimental interpretation and atomistic simulations is likely to be due to a difference in the definition of the clusters. In Figure 15, clusters are defined through a series of hydrogen-bonded water molecules, which implicitly includes the concept of connectivity. On the other hand, Zimm−Lundberg theory is based on the *cluster function*, originally introduced by Kirkwood and Buff,[175] which compares the environment of a water molecule in the polymer with respect to that expected of a homogeneous distribution.[27] This statistical function indicates relative densities of water molecules but not physical clusters. Indeed, Figure 16 shows that cluster geometries are not trivial and that they are actually closer to chains or open networks of water molecules rather than to dense droplets. At the higher percentages, it even approaches a cocontinuous network, similar to what has been seen in some other atomistic simulations of polymers in water.[36,38,42,44,51,60]

The average mean square radii of gyration of the clusters $\langle S^2_{clust}\rangle$ are displayed as a function of cluster size and water content in Figure 17. The linear increase of $\langle S^2_{clust}\rangle$ confirms that the clusters systematically tend to adopt linear or open network geometries rather than globular ones, with the latter implying an increase in $\langle S^2_{clust}\rangle$ proportional to a power of 2/3 in the cluster size. In fact, in the limit that globular clusters have a uniform density given by that of bulk liquid water, it is simple to show that

$$\langle S^2_{clust}\rangle \approx \frac{3}{5}\left(\frac{3Nm}{4\pi\rho}\right)^{\frac{2}{3}} \tag{7}$$

where N is the number of molecules in the cluster and m is the mass of a water molecule. This line is also drawn in Figure 17 using a density of 958.05 kg/m^3, that is, that of liquid water at 373 K. Also drawn in Figure 17 are the results obtained for the as-inserted water molecules. Values of the mean square radii of gyration of clusters in this latter case fall between the relaxed MD values and those of the globular limit. This again suggests a certain rearrangement of the cluster distribution once the water is allowed to relax.

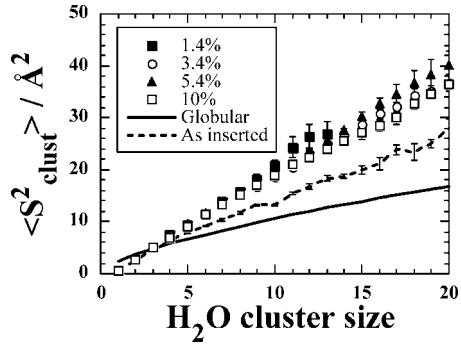

Figure 17. $\langle S^2_{clust} \rangle$ for the water clusters as a function of cluster size. Results are averaged over five systems for each water content, and their standard errors are displayed. The line represents the theoretical values for globular clusters based on the expression given in eq 7. The dashed line gives the results obtained from the as-inserted water molecules.

These nonspherical geometries have also clearly been characterized in other simulation studies.[34,60,61] In addition, linear or open network clusters do not give rise to such a high local density of water molecules, which could explain the discrepancy between the experimental interpretation of the Zimm−Lundberg cluster function and the actual presence of clusters. It should also be noted that the experimental solubility curves are obtained through macroscopic weighing techniques, which are subject to large errors for low activities. As far as other experimental techniques are concerned, the models are consistent with the dielectric measurements of Xu et al. where Kapton films containing water revealed a characteristic double-loss peak.[28] Its two components, which are also seen in the ^{2}H NMR spectra, were originally designated as γ_1 and γ_2. They were attributed, respectively, to sites where isolated water molecules are loosely coupled to the polymer chains (γ_1) and clusters of water molecules (γ_2). Since NMR ruled out the possibility of small liquidlike droplets, it was postulated that those clusters probably consisted of small chains of molecules.[28] The results of Xu et al. were confirmed in other studies using either dielectric relaxation or NMR spectroscopies.[25,29,30] It was further shown that the D_2O molecules in the γ_2 sites exhibit a preferred orientation perpendicular to the plane of the film,[30] and that the dipole moment associated with the γ_2 relaxation is very large,[25] which is also consistent with chains of small molecules. While it is not always easy to separate both contributions because of the large overlap of both peaks, the γ_2 component is found in an attenuated form at water percentages as low as 1.6[28,30] or 1.1 wt %[25] and increases rapidly with the total moisture uptake. In addition, its large width is indicative of a wide range of cluster sizes and configurations.[25] This strongly supports the findings of the atomistic models. This is also the case for the infrared ATR characterization of Van Alsten et al. where the vibrational spectra show a bimodal distribution and where ~77% of water is presumed to be in an aggregated form at 303 K and at saturation.[31] This estimation is in good agreement with our model average percentage of water molecules being found in clusters, which is ~84% at 373 K for the 3.4% systems.

5. Conclusions

Fully atomistic MD simulations of dry and hydrated Kapton have been successfully carried out on more than 40 model systems. The pure polymer matrices were prepared using the efficient hybrid PMC-MD single-chain sampling technique, following the validation of the local energy parameter $n_{bonds} = 4$. No significant distortion of the chains on the intermediate length scales related to the introduction of the excluded volume potential was observed. Dry Kapton models were all found to be in good agreement with experimental data in terms of densities, Hildebrand solubility parameters, conformational properties, and free volume fractions at both 300 and 373 K. In addition to validating the force field, it was also established that the generation procedure is highly reproducible.

Simulations at different weight percentages of water at 373 K consistently show that the polymer matrices prepared here only start to swell for water contents above ~3% wt. In addition, even at 10% wt water content, the model volumes and interaction energies of the Kapton chains and the water penetrants are not simply additive. Local relaxation of the polymer induced by water is confirmed by the molecular distances and the probe accessible volume distribution of the matrix with a tendency for more small holes at 8% and 10% wt water.

At low water contents, ~75% of water molecules are H-bonded to the hydrophilic sites on the polymer chains, principally to the more numerous, more attractive, and more accessible carbonyl oxygens O_{carb} and, to a lesser extent, to the ether oxygens O_{eth}. Wherever possible, water molecules prefer to be H-bonded to a second hydrophilic site and, in many cases, this is another water molecule. Indeed, these water bridges occur not only between two polymer sites but, more often, between two water molecules or between one polymer site and one water molecule. Despite the excess of hydrophilic sites on the polymer chain, coordination to the chain is progressively less favorable than coordination to another water at higher concentrations. Our simulations suggest that the hypothesis of "inaccessible" hydrophilic sites on the polymer chain is unfounded as the cumulative number of carbonyl and ether oxygens visited steadily increases. Furthermore, the H-bonding network fluctuates, with typical correlation times τ being in the range of 10^2-10^3 ps. As expected, the continuous H-bond lifetimes τ_c are much shorter, that is, <1 ps. However, up to ~10% wt water, both τ and τ_c in Kapton are relatively insensitive to the concentration.

Water clusters have been found to be present even at the lowest concentrations, in agreement with certain experimental findings. The discrepancy between the commonly used interpretation of the solubility curves based on the Zimm−Lundberg theory and the presence of clusters in the water range studied can be explained by the geometries of the clusters. They are clearly much closer to chains or open networks of water molecules rather than to dense droplets.

Water solubilities have not been reported in this paper, as initial tests with the Widom test-particle insertion method[81] gave values with very large error bars. It is thus intended to couple this technique with the grid-search calculation.[69,82] This should be the subject of a future publication, along with the analyses of water diffusion in Kapton. Furthermore, in order to assess whether the results presented here can be extended to other polymers with the same type of uptake curves, similar investigations are currently being carried out on long-chain polysulfones, for which experimental data is also available.[13] It would also be interesting to study other polyimides, where it is well-known that both chemical structure and morphology can affect water-sorption behavior.[32]

Acknowledgment. This work was funded by the joint "COPOLA" (COmposite and POLymer Ageing) research program involving EDF, NEXANS France, LABORELEC, the CEA, the INRA, and the CNRS. "COPOLA" is also thanked for its scientific contribution. We gratefully acknowledge the University of Savoie and EDF for the provision of computer time.

References and Notes

(1) Verdu, J. *Sci. Tech. Ingénieur* **1985**, *A3165*, 1–6.
(2) Han, S. O.; Drzal, L. T. *Eur. Polym. J.* **2003**, *39* (9), 1791–1799.

(3) Belluci, F.; Khamis, I.; Senturia, S. D.; Latanision, R. M. *J. Electrochem. Soc.* **1990**, *137* (6), 1778–1784.
(4) Deligöz, H.; Yalcinyuva, T.; Özgümüs, S.; Yildirim, S. *J. Appl. Polym. Sci.* **2006**, *100* (1), 810–818.
(5) Jacobson, P. A.; Rosa, L. G.; Kraemer, K.; Ducharme, S.; Dowben, P. A. *Mater. Lett.* **2007**, *61* (4–5), 1137–1141.
(6) Baschek, G.; Hartwig, G.; Zahradnik, F. *Polymer* **1999**, *40* (12), 3433–3441.
(7) Merdas, I.; Thominette, F.; Verdu, J. *J. Appl. Polym. Sci.* **2000**, *77* (7), 1445–1451.
(8) Kim, H. J.; Seo, D. W. *Int. J. Fatigue* **2006**, *28* (10), 1307–1314.
(9) Dhakal, H. N.; Zhang, Z. Y.; Richardson, M. O. W. *Compos. Sci. Technol.* **2007**, *67* (7–8), 1674–1683.
(10) Adamson, M. J. *J. Mater. Sci.* **1980**, *15* (7), 1736–1745.
(11) Van Krevelen, D. W. *Properties of polymers: their correlation with chemical structure; their numerical estimation and prediction from additive group contributions*, 3rd completely revised ed.; Elsevier: Amsterdam, 1990.
(12) Barton, A. F. M. *Handbook of solubility and other cohesion parameters*, 2nd ed.; CRC Press: Boca Raton, FL, 1983.
(13) Gaudichet-Maurin, E. Caractérisation et vieillissement d'une membrane d'ultrafiltration d'eau. Ph.D. Thesis, ENSAM, Paris, 2005.
(14) Puffr, R.; Sebenda, J. *J. Polym. Sci., Part C: Polym. Symp.* **1967**, *16*, 79–93.
(15) Starkweather, H. W. *Macromolecules* **1975**, *8* (4), 476–479.
(16) Han, H.; Gryte, C. C.; Ree, M. *Polymer* **1995**, *36* (8), 1663–1672.
(17) Yang, D. K.; Koros, W. J.; Hopfenberg, H. B.; Stannett, V. T. *J. Appl. Polym. Sci.* **1985**, *30* (3), 1035–1047.
(18) Yang, D. K.; Koros, W. J.; Hopfenberg, H. B.; Stannett, V. T. *J. Appl. Polym. Sci.* **1986**, *31* (6), 1619–1629.
(19) Barrie, J. A.; Sagoo, P. S.; Johncock, P. *J. Appl. Polym. Sci.* **1987**, *33* (6), 2253–2258.
(20) Okamoto, K.-I.; Tanihara, N.; Watanabe, H.; Tanaka, K.; Kita, H.; Nakamura, A.; Kusuki, Y.; Nakagawa, K. *J. Polym. Sci., Part B: Polym. Phys.* **1992**, *30*, 1223–1231.
(21) Larobina, D.; Lavorgna, M.; Mensitieri, G.; Musto, P.; Vautrin, A. *Macromol. Symp.* **2007**, *247* (1), 11–20.
(22) Hubbel, W. H., Jr.; Brandt, H.; Munir, Z. A. *J. Polym. Sci., Polym. Phys. Ed.* **1975**, *13*, 493–507.
(23) Sacher, E.; Susko, J. R. *J. Appl. Polym. Sci.* **1979**, *23* (8), 2355–2364.
(24) Pranjoto, H.; Denton, D. D. *J. Appl. Polym. Sci.* **1991**, *42*, 75–83.
(25) Lim, B. S.; Nowick, A. S.; Lee, K.-W.; Viehbeck, A. *J. Polym. Sci., Part B: Polym. Phys.* **1993**, *31*, 545–555.
(26) Ree, M.; Han, H.; Gryte, C. C. *High Perform. Polym.* **1994**, *6*, 321–333.
(27) Zimm, B.; Lundberg, J. L. *J. Phys. Chem.* **1956**, *60* (4), 425–428.
(28) Xu, G.; Gryte, C. C.; Nowick, A. S.; Li, S. Z.; Pak, Y. S.; Greenbaum, S. G. *J. Appl. Phys.* **1989**, *66* (11), 5290–5296.
(29) Li, S. Z.; Pak, Y. S.; Adamic, K.; Greenbaum, S. G.; Lim, B. S.; Xu, G.; Nowick, A. S. *J. Electrochem. Soc.* **1992**, *139* (3), 662–667.
(30) Li, S. Z.; Chen, R. S.; Greenbaum, S. G. *J. Polym. Sci., Part B: Polym. Phys.* **1995**, *33*, 403–409.
(31) Van Alsten, J. G.; Coburn, J. C. *Macromolecules* **1994**, *27* (14), 3746–3752.
(32) Seo, J.; Lee, A.; Lee, C.; Han, H. *J. Appl. Polym. Sci.* **2000**, *76*, 1315–1323.
(33) Knopp, B.; Suter, U. W. *Macromolecules* **1997**, *30* (20), 6114–6119.
(34) Goudeau, S.; Charlot, M.; Vergelati, C.; Müller-Plathe, F. *Macromolecules* **2004**, *37* (21), 8072–8081.
(35) Goudeau, S.; Charlot, M.; Müller-Plathe, F. *J. Phys. Chem. B* **2004**, *108* (48), 18779–18788.
(36) Netz, P. A.; Dorfmüller, T. *J. Phys. Chem. B* **1998**, *102* (25), 4875–4886.
(37) Kotelyanskii, M. J.; Wagner, N. J.; Paulaitis, M. E. *J. Membr. Sci.* **1998**, *139*, 1–16.
(38) Kotelyanskii, M. J.; Wagner, N. J.; Paulaitis, M. E. *Comput. Theor. Polym. Sci.* **1999**, *9*, 301–306.
(39) Tönsing, T.; Oldiges, C. *Phys. Chem. Chem. Phys.* **2001**, *3*, 5542–5549.
(40) Bharadwaj, R. K. *Macromolecules* **2002**, *35* (13), 5334–5336.
(41) Nick, B.; Suter, U. W. *Comput. Theor. Polym. Sci.* **2001**, *11*, 49–55.
(42) Tamai, Y.; Tanaka, H.; Nakanishi, K. *Macromolecules* **1996**, *29* (21), 6750–6760.
(43) Tamai, Y.; Tanaka, H.; Nakanishi, K. *Macromolecules* **1996**, *29* (21), 6761–6769.
(44) Tamai, Y.; Tanaka, H. *Mol. Simul.* **1999**, *21*, 283–301.
(45) Müller-Plathe, F.; Van Gunsteren, W. F. *Polymer* **1997**, *38* (9), 2259–2268.
(46) Müller-Plathe, F. *Macromolecules* **1998**, *31* (19), 6721–6723.
(47) Müller-Plathe, F. *J. Chem. Phys.* **1998**, *108* (19), 8252–8263.
(48) Müller-Plathe, F. *J. Membr. Sci.* **1998**, *141* (2), 147–154.
(49) Karlsson, G. E.; Johansson, T. S.; Gedde, U. W.; Hedenqvist, M. S. *J. Macromol. Sci., Phys.* **2002**, *B41* (2), 185206.
(50) Kucukpinar, E.; Doruker, P. *Polymer* **2004**, *45*, 3555–3564.
(51) Tasaki, K. *J. Am. Chem. Soc.* **1996**, *118* (35), 8459–8469.
(52) Heymann, B.; Grubmüller, H. *Chem. Phys. Lett.* **1999**, *307*, 425–432.
(53) Smith, G. D.; Bedrov, D.; Borodin, O. *Phys. Rev. Lett.* **2000**, *85* (26), 5583–5586.
(54) Smith, G. D.; Bedrov, D.; Borodin, O. *J. Am. Chem. Soc.* **2000**, *122* (39), 9548–9549.
(55) Borodin, O.; Bedrov, D.; Smith, G. D. *J. Phys. Chem. B* **2002**, *106* (20), 5184–5193.
(56) Borodin, O.; Bedrov, D.; Smith, G. D. *J. Phys. Chem. B* **2002**, *106* (20), 5194–5199.
(57) Ennari, J.; Elomaa, M.; Sundholm, F. *Polymer* **1999**, *40*, 5035–5041.
(58) Ennari, J.; Neelov, I.; Sundholm, F. *Polymer* **2004**, *45*, 4171–4179.
(59) Kim, W.-K.; Mattice, W. L. *Macromolecules* **1998**, *31* (26), 9337–9344.
(60) Elliott, J. A.; Hanna, S.; Elliott, A. M. S.; Cooley, G. E. *Phys. Chem. Chem. Phys.* **1999**, *1*, 4855–4863.
(61) Elliott, J. A.; Paddison, S. J. *Phys. Chem. Chem. Phys.* **2007**, *9*, 2602–2618.
(62) Pozuelo, J.; Riande, E.; Saiz, E.; Compan, V. *Macromolecules* **2006**, *39* (25), 8862–8866.
(63) Hu, N.; Chen, R.; Hsu, A. *Polym. Int.* **2006**, *55*, 872–882.
(64) Allen, R.; Bandyopadhyay, S.; Klein, M. L. *Langmuir* **2000**, *16* (26), 10547–10552.
(65) Bandyopadhyay, S.; Tarek, M.; Lynch, M. L.; Klein, M. L. *Langmuir* **2000**, *16* (3), 942–946.
(66) Abel, S.; Waks, M.; Marchi, M.; Urbach, W. *Langmuir* **2006**, *22* (22), 9112–9120.
(67) Fukuda, M.; Kuwajima, S. *J. Chem. Phys.* **1998**, *108* (7), 3001–3009.
(68) Fukuda, M. *J. Chem. Phys.* **1998**, *109* (15), 6476–6485.
(69) Dömötör, G.; Hentschke, R. *Macromol. Theory Simul.* **2004**, *13*, 506–511.
(70) Mijovic, J.; Zhang, H. *J. Phys. Chem. B* **2004**, *108* (8), 2557–2563.
(71) Wu, C.; Xu, W. *Polymer* **2007**, *48*, 5440–5448.
(72) Pawloski, A. R.; Torres, J. A.; Nealey, P. F.; De Pablo, J. J. *J. Vac. Sci. Technol., B* **1999**, *17* (6), 3371–3378.
(73) Chen, Z.; Gu, Q.; Zou, H.; Zhao, T.; Wang, H. *J. Polym. Sci., Part B: Polym. Phys.* **2007**, *45*, 884–891.
(74) Entrialgo-Castano, M.; Lendlein, A.; Hofmann, D. *Adv. Eng. Mater.* **2006**, *8* (5), 434–439.
(75) Cheng, Y.-K.; Rossky, P. J. *Nature* **1998**, *392*, 696–699.
(76) Mazur, A. K. *J. Am. Chem. Soc.* **2002**, *124* (49), 14707–14715.
(77) Pal, S.; Maiti, P. K.; Bagchi, B. *J. Phys.: Condens. Matter* **2005**, *17*, S4317–S4331.
(78) Knopp, B.; Suter, U. W.; Gusev, A. A. *Macromolecules* **1997**, *30*, 6107–6113.
(79) Fukuda, M. *J. Chem. Phys.* **2000**, *112* (1), 478–486.
(80) Tamai, Y.; Tanaka, H.; Nakanishi, K. *Macromolecules* **1995**, *28* (7), 2544–2554.
(81) Widom, B. *J. Chem. Phys.* **1963**, *39*, 2808–2812.
(82) Dömötör, G.; Hentschke, R. *J. Phys. Chem. B* **2004**, *108* (7), 2413–2417.
(83) Poon, T. W.; Silverman, B. D.; Saraf, R. F.; Rossi, A. R.; Ho, P. S. *Phys. Rev. B: Condens. Matter Mater. Phys.* **1992**, *46* (18), 11456–11462.
(84) Tiller, A. R. *Macromolecules* **1992**, *25* (18), 4605–4611.
(85) Neyertz, S.; Brown, D.; Douanne, A.; Bas, C.; Albérola, N. D. *J. Phys. Chem. B* **2002**, *106*, 4617–4631.
(86) Ramos, M.-M. D. *Vacuum* **2002**, *64* (3–4), 255–260.
(87) Heuchel, M.; Hofmann, D. *Desalination* **2002**, *144*, 67–72.
(88) Heuchel, M.; Hofmann, D.; Pullumbi, P. *Macromolecules* **2004**, *37*, 201–214.
(89) McKechnie, J. I.; Brown, D.; Clarke, J. H. R. *Macromolecules* **1992**, *25*, 1562–1567.
(90) Hofmann, D.; Fritz, L.; Ulbrich, J.; Paul, D. *Comput. Theor. Polym. Sci.* **2000**, *10*, 419–436.
(91) Neyertz, S. *Soft Mater.* **2007**, *4* (1), 15–83.
(92) Brown, D.; Clarke, J. H. R.; Okuda, M.; Yamazaki, T. *J. Chem. Phys.* **1994**, *100* (2), 1684–1692.
(93) Brown, D.; Clarke, J. H. R.; Okuda, M.; Yamazaki, T. *J. Chem. Phys.* **1994**, *100*, 6011–6018.
(94) Brown, D.; Clarke, J. H. R.; Okuda, M.; Yamazaki, T. *J. Chem. Phys.* **1996**, *104* (5), 2078–2082.
(95) Neyertz, S.; Brown, D. *J. Chem. Phys.* **1995**, *102* (24), 9725–9735.
(96) Neyertz, S.; Brown, D. *J. Chem. Phys.* **1996**, *104* (24), 10063.
(97) Neyertz, S.; Brown, D.; Clarke, J. H. R. *J. Chem. Phys.* **1996**, *105* (5), 2076–2088.
(98) Neyertz, S.; Brown, D. *J. Chem. Phys.* **2001**, *115* (2), 708–717.
(99) Neyertz, S.; Brown, D. *Macromolecules* **2004**, *37* (26), 10109–10122.

(100) Pinel, E.; Brown, D.; Bas, C.; Mercier, R.; Albérola, N. D.; Neyertz, S. *Macromolecules* **2002**, *35*, 1019810209.
(101) Neyertz, S.; Douanne, A.; Brown, D. *Macromolecules* **2005**, *38* (24), 10286–10298.
(102) Neyertz, S.; Douanne, A.; Brown, D. *J. Membr. Sci.* **2006**, *280*, 517–529.
(103) Neyertz, S. *Macromol. Theory Simul.* **2007**, *16*, 513–524.
(104) Hammonds, K. D.; Ryckaert, J.-P. *Comput. Phys. Commun.* **1991**, *62*, 336–351.
(105) Ewald, P. P. *Ann. Phys.* **1921**, *64*, 253–287.
(106) Smith, W. *Comput. Phys. Commun.* **1992**, *67*, 392.
(107) Clark, M.; Cramer, R. D., III; Van Opdenbosch, N. *J. Comput. Chem.* **1989**, *10* (8), 982–1012.
(108) Frisch, M. J.; Trucks, G. W.; Schlegel, H. B.; Scusera, G. E.; Robb, M. A.; Cheeseman, J. R.; Zakrzewski, V. G.; Montgomery J. A., Jr.; Stratmann, R. E.; Burant, J. C.; Dapprich, S.; Millam, J. M.; Daniels, A. D.; Kudin, K. N.; Strain, M. C.; Farkas, O.; Tomasi, J.; Barone, V.; Cossi, M.; Cammi, R.; Mennucci, B.; Pomelli, C.; Adamo, C.; Clifford, S.; Ochterski, J.; Petersson, G. A.; Ayala, P. Y.; Cui, Q.; Morokuma, K.; Malick, D. K.; Rabuck, A. D.; Raghavachari, K.; Foresman, J. B.; Cioslowski, J.; Ortiz, J. V.; Baboul, A. G.; Stefanov, B. B.; Liu, G.; Liashenko, A.; Piskorz, P.; Komaromi, I.; Gomperts, R.; Martin, R. L.; Fox, D. J.; Keith, T.; Al-Laham, M. A.; Peng, C. Y.; Nanayakkara, A.; Gonzalez, C.; Challacombe, M.; Gill, P. M. W., Johnson, B.; Chen, W.; Wong, M. W.; Andres, J. L.; Gonzalez, C.; Head-Gordon, M.; Replogle, E. S.; Pople, J. A. *Gaussian 98*; Gaussian Inc.: Pittsburgh, PA, 1998.
(109) Berendsen, H. J. C.; Grigera, J. R.; Straatsma, T. P. *J. Phys. Chem.* **1987**, *91*, 6269.
(110) Heyes, D. M. *J. Chem. Soc., Faraday Trans.* **1994**, *90* (20), 3039–3049.
(111) Guillot, B. *J. Mol. Liq.* **2002**, *101* (1–3), 219–260.
(112) Zhang, Z.; Duan, Z. *Phys. Earth Planet. Inter.* **2005**, *149*, 335–354.
(113) Allen, M. P.; Tildesley, D. J. *Computer Simulation of Liquids*; Clarendon Press: Oxford, England, 1987.
(114) Brown, D. *The gmq User Manual*, version 3; available at http://www.lmops.univ-savoie.fr/brown/gmq.html, **1999**.
(115) Marceau, S. Architecture Multiéchelle et Propriétés Mécaniques de Nanocomposites. Ph.D. Thesis, University of Savoie, Bourget-du-Lac, 2003. Available at http://www.lmops.univ-savoie.fr/people/smarceau/.
(116) Queyroy, S. Simulations moléculaires dynamiques de surfaces de polymère amorphe: cas de la cellulose. University of Savoie, France, Bourget-du-Lac, 2004.
(117) Lal, M. *Mol. Phys.* **1969**, *17* (1), 57–64.
(118) Madras, N.; Sokal, A. *J. Stat. Phys.* **1988**, *50* (1–2), 109–186.
(119) Flory, P. J. *The Statistical Mechanics of Chain Molecules*; Hanser Publishers: New York, 1988.
(120) Brown, D.; Clarke, J. H. R. *Comput. Phys. Commun.* **1991**, *62*, 360–369.
(121) Berendsen, H. J. C.; Postma, J. P. M.; Van Gunsteren, W. F.; DiNola, A.; Haak, J. R. *J. Chem. Phys.* **1984**, *81*, 3684–3690.
(122) Brown, D.; Neyertz, S. *Mol. Phys.* **1995**, *84* (3), 577–595.
(123) Fincham, D. *Mol. Simul.* **1994**, *13*, 1–19.
(124) Vora, H. R.; Goh, S. H.; Chung, T.-S. *Polym. Eng. Sci.* **2000**, *40* (6), 1318–1329.
(125) Hasegawa, M.; Horie, K. *Prog. Polym. Sci.* **2001**, *26*, 259–335.
(126) Stern, S. A.; Mi, Y.; Yamamoto, H. *J. Polym. Sci., Part B: Polym. Phys.* **1989**, *27*, 1887–1909.
(127) Park, J. Y.; Paul, D. R. *J. Membr. Sci.* **1997**, *125*, 23–39.
(128) Niyogi, S.; Adhikari, B. *Eur. Polym. J.* **2002**, *38* (6), 1237–1243.
(129) Ronova, I. A.; Rozhkov, E. M.; Alentiev, A. Y.; Yampolskii, Y. P. *Macromol. Theory Simul.* **2003**, *12*, 425–439.
(130) Hofmann, D.; Heuchel, M.; Yampolskii, Y.; Khotimskii, V.; Shantarovich, V. *Macromolecules* **2002**, *35*, 2129–2140.
(131) Auhl, R.; Everaers, R.; Grest, G. S.; Kremer, K.; Plimpton, S. J. *J. Chem. Phys.* **2003**, *119*, 12718–12728.
(132) Pottinger, M. L.; Coburn, J. C.; Edman, J. R. *J. Polym. Sci., Part B: Polym. Phys.* **1994**, *32*, 825–837.
(133) Hoy, K. L. *J. Paint Technol.* **1970**, *42*, 76.
(134) Fedors, R. F. *Polym. Eng. Sci.* **1974**, *14*, 147–154.
(135) Bas, C.; Mercier, R.; Sanchez-Marcano, J.; Neyertz, S.; Albérola, N. D.; Pinel, E. *J. Polym. Sci., Part B: Polym. Phys.* **2005**, *43*, 2413–2426.
(136) Kim, T. H.; Koros, W. J.; Husk, G. R.; O'Brien, K. C. *J. Membr. Sci.* **1988**, *37*, 45–62.
(137) LaFemina, J. P.; Arjavalingam, G.; Houghman, G. *J. Chem. Phys.* **1989**, *90*, 5154.
(138) Kotov, B. V. *Russ. J. Phys. Chem.* **1988**, *62* (10), 1408–1417.
(139) Ghosh, M. K.; Mittal, K. L. *Polyimides: fundamentals and applications*; Marcel Dekker, Inc.: New York, 1996.
(140) Kitano, Y.; Usami, I.; Obata, Y.; Okuyama, K.; Jinda, T. *Polymer* **1995**, *36* (6), 1123–1126.
(141) Bondi, A. *Physical Properties of Molecular Crystals, Liquids and Gases*; John Wiley & Sons: New York, 1968.
(142) Brusa, R. S.; Dupasquier, A.; Galvanetto, E.; Zecca, A. *Appl. Phys.* **1992**, *A54*, 233–238.
(143) Schmitz, H.; Müller-Plathe, F. *J. Chem. Phys.* **2000**, *112* (2), 1040–1045.
(144) Kruse, J.; Kanzow, J.; Rätzke, K.; Faupel, F.; Heuchel, M.; Frahn, J.; Hofmann, D. *Macromolecules* **2005**, *38* (23), 9638–9643.
(145) Boyd, R. H.; Pant, P. V. K. *Macromolecules* **1991**, *24* (14), 4078–4083.
(146) Pant, P. V. K.; Boyd, R. H. *Macromolecules* **1993**, *26* (4), 679–686.
(147) Lee, S.; Mattice, W. L. *Comput. Theor. Polym. Sci.* **1999**, *9*, 57–61.
(148) Nagel, C.; Schmidtke, E.; Günther-Schade, K.; Hofmann, D.; Fritsch, D. *Macromolecules* **2000**, *33*, 2242–2248.
(149) Pinel, E.; Bas, C.; Neyertz, S.; Albérola, N. D.; Petiaud, R.; Mercier, R. *Polymer* **2002**, *43*, 1983–1992.
(150) Moylan, C. R.; Best, M. E.; Ree, M. *J. Polym. Sci., Part B: Polym. Phys.* **1991**, *29*, 87–92.
(151) Belluci, F.; Nicodemo, L. *Corrosion* **1993**, *49* (3), 235–247.
(152) Han, H.; Seo, J.; Ree, M.; Pyo, S. M.; Gryte, C. C. *Polymer* **1998**, *39* (13), 2963–2972.
(153) Han, H.; Chung, H.; Gryte, C. C.; Shin, T. J.; Ree, M. *Polymer* **1999**, *40*, 2681–2685.
(154) Lee, C.; Shul, Y.; Han, H. *J. Polym. Sci., Part B: Polym. Phys* **2002**, *40*, 2190–2198.
(155) Giacomelli Penon, M.; Picken, S. J.; Wübbenhorst, M.; De Vos, G.; Van Turnhout, J. *Rev. Sci. Instrum.* **2006**, *77*, 115107-1–115107-6.
(156) Merdas, I.; Tcharkhtchi, A.; Thominette, F.; Verdu, J.; Dean, K.; Cook, W. *Polymer* **2002**, *43*, 4619–4625.
(157) Merdas, I.; Thominette, F.; Tcharkhtchi, A.; Verdu, J. *Compos. Sci. Technol.* **2002**, *62*, 487–492.
(158) Blumentritt, B. F. *Polym. Eng. Sci.* **1978**, *18* (16), 1216–1219.
(159) Jou, J.-H.; Huang, R.; Huang, P.-T.; Shen, W.-P. *J. Appl. Polym. Sci.* **1991**, *43* (5), 857–875.
(160) Kirchheim, R. Private communication, **2007**.
(161) Rowe, B. W.; Freeman, B. D.; Paul, D. R. *Macromolecules* **2007**, *40* (8), 2806–2813.
(162) Miyagi, Z.; Tanaka, K. *Polymer* **1975**, *16* (6), 441–444.
(163) Stober, E. J.; Seferis, J. C.; Keenan, J. D. *Polymer* **1984**, *25* (12), 1845–1852.
(164) Hernandez, R. J.; Giacin, J. R.; Grulke, E. A. *J. Membr. Sci.* **1992**, *65* (1–2), 187–199.
(165) Hu, Y. S.; Mehta, S.; Schiraldi, D. A.; Hiltner, A.; Baer, E. *J. Polym. Sci., Part B: Polym. Phys.* **2005**, *43*, 1365–1381.
(166) Benczédi, D.; Tomka, I.; Escher, F. *Macromolecules* **1998**, *31* (9), 3055–3061.
(167) Ania, F.; Dunkel, M.; Bayer, R. K.; Balta-Calleja, F. J. *J. Appl. Polym. Sci.* **2002**, *85*, 1246–1252.
(168) Watari, T.; Fang, J.; Tanaka, K.; Kita, H.; Okamoto, K.-I.; Hirano, T. *J. Membr. Sci.* **2004**, *230* (1–2), 111–120.
(169) Borodin, O.; Bedrov, D.; Smith, G. D. *Macromolecules* **2001**, *34* (16), 5687–5693.
(170) Waters, J. F.; Likavec, W. R.; Ritchey, W. M. *J. Appl. Polym. Sci.* **1994**, *53*, 59–70.
(171) Pimentel, G. C.; McClellan, A. L. *The Hydrogen Bond*; W. H. Freeman: San Francisco, 1960.
(172) Rapaport, D. C. *Mol. Phys.* **1983**, *50* (5), 1151–1162.
(173) Stillinger, F. H. *Adv. Chem. Phys.* **1975**, *31*, 1–101.
(174) Lanczos, C. *SIAM J. Numer. Anal.* **1964**, *B1*, 86–96.
(175) Kirkwood, J. G.; Buff, F. P. *J. Chem. Phys.* **1951**, *19* (6), 774–777.
(176) Humphrey, W.; Dalke, A.; Schulten, K. *J. Mol. Graphics* **1996**, *14* (1), 33–38.

MA702173J